Effective plasmonic coupling and propagation facilitates ultrasensitive and remote sensing using Surface Enhanced Raman Spectroscopy

Collins Nganou,[a] Andrew J. Carrier,[a] Dongchang Yang,[a] Yongli Chen,[b] Naizhen Yu,[a] Doug Richards,[a] Craig Bennett,[c] Ken Oakes,[d] Stephanie L. MacQuarrie,[a] and Xu Zhang*[a]

[a]Department of Chemistry, Cape Breton University, Sydney, Nova Scotia, B1P 6L2, Canada

[b]Postdoctoral Innovation Practice Base, Shenzhen Polytechnic, Shenzhen, 518055, China

[c]Department of Physics, Acadia University, Wolfville, Nova Scotia, B4P 2R6, Canada

[d]Department of Biology, Cape Breton University, Sydney, Nova Scotia, B1P 6L2, Canada

*Corresponding Author. E-mail: Xu_Zhang@cbu.ca

Abstract

Surface-enhanced Raman spectroscopy (SERS) is a sensitive technique for the detection of analytes through light scattering that is enhanced by chemical and electromagnetic effects through interactions on surfaces, particularly in nano-gaps. Herein we show that dissolved oxygen is the strongest attenuator of the SERS response in aqueous solution and its removal by chemical means can lower the detection limit by 10^9–10^{10} times, to achieve unprecedented sensitivity, i.e., detection of a single molecule in ~300 μL of sample solution. It also enables remote detection of the analyte outside of the field of view of the incident laser beam, e.g., over a distance of 1 m, which we propose is due to the coupling of the plasmonic field within and between nanoparticle aggregates, allowing for signal transmission throughout the sample volume.

Introduction

The development of an affordable and portable instrument for ultrasensitive and specific *in situ* detection of extremely low concentrations of analyte molecules in aqueous samples is highly challenging.[1-6] Surface-enhanced Raman spectroscopy (SERS)[7,8] is a promising technology to achieve this goal because of its high sensitivity, i.e., up to one single molecule within the detector's field of view (single molecule SERS, or SM-SERS),[9,10] non-destructivity, label-free detection, and portability. The sensitivity and reproducibility of SERS measurements have been significantly improved because of the rapid development of nanotechnology over the last two decades, for instance via engineering

optical hot spots.[11,12] Hot spots are locations on nanostructures exhibiting the strongest electromagnetic field on the substrate; they are normally located on high-curvature regions, such as nanoprism tips, or within nano-gaps of $\leqslant$10 nm distance between neighboring nanoparticles.[13,14] Hot spots are believed to generate the highest signal amplification for SERS.[15] However, the sensitivity of SM-SERS is still limited because the analyte molecule must be located simultaneously within a hot spot, in the sampling area of the Raman laser beam, and in the field of view of the optical fiber that collects the scattered light to be detectable. This sampling area or volume is normally a very small or is even a negligible fraction of the whole sample volume.[16] Therefore, the detection limit of SM-SERS in practice is at the nM or pM level (10^{-9}–10^{-12} M).[16,17] Recently, an approach was reported to break this limit by coupling SERS detection with the pre-concentration of analytes using super-hydrophobic or omniphobic surfaces, which greatly increased the detection sensitivity down to fM levels.[17,18]

A different approach was to study the factors that affect the detection limit of SERS. One important factor is the surface oxidation of the SERS substrate.[19] For example, when silver nanoparticles (AgNPs) or silver films, commonly used SERS substrates, are oxidized by oxygen or the ppb level of ozone existing in ambient air to form a sub-monolayer of Ag_2O,[19] the SERS enhancement factors (EFs) decrease by five orders of magnitude. Such a decrease is analyte-dependent and correlated quantitatively to the thickness of the Ag_2O layer.[20-22] The effect of the Ag_2O layer was attributed to a decrease in both analyte adsorption and the metal-to-analyte electron transfer, compromising both the chemical and electromagnetic enhancement of SERS.[23] However, the effect of

substrate oxidation on SERS EFs was later observed to be less significant;[24,25] although together with atmospheric carbon contamination the noise level increased with simultaneously decreasing signal intensity.[25] In addition, it was discovered that SERS detection could be achieved even using AuNPs coated with a thin layer of silica or alumina as the substrate, i.e., shell-isolated nanoparticle-enhanced Raman spectroscopy (SHINERS). The success of SHINERS indicates that a thin layer of dielectric oxide on AuNPs does not result in a drastic decrease of SERS EFs.[11,26]

After careful examination of the previous work, we found that although the role of dissolved oxygen (DO) in aqueous samples was examined through inert gas (Ar) sparging,[21] which resulted in significant sensitivity enhancement, this was still insufficient to lower the DO concentration to levels where SERS EFs were completely unattenuated.[21] We achieved unprecedented SERS sensitivity by using various chemical oxygen scavengers, obtaining zM level analyte detection in aqueous samples. Furthermore, remote sensing of the analyte was realized; this discovery may bring radical insight into the field of single molecule detection regarding instrument development, analytical applications, and the fundamental understanding of the SERS technique.

Results and Discussion

Basic experimental conditions

Silver nanoplatelets (AgNPs) stabilized by small loosely bound capping molecules, i.e., citrate and ethanol, were used as the SERS substrate because of their excellent optical

properties[27] and the ease of displacement of the capping ligands by the thiolated analytes. These AgNPs were prepared using an established literature method[27] and their size, morphology, and optical properties were characterized using UV-Vis spectroscopy, transmission electron microscopy, and dynamic light scattering (see Figs. S1 and S2). The main analytes used were thiophenols, i.e., p-aminothiophenol (pATP) and p-nitrothiophenol (pNTP), because of their strong adsorption to the AgNPs substrate and distinct SERS spectra (Raman spectra in Fig. S3.). The spectral window observed was generally limited to those wavenumbers $\geqslant$1000 cm^{-1} because of overpowering signals generated by the AgNP capping agents, citrate and ethanol, under 1000 cm^{-1} (see Fig. S4). Dissolved oxygen was removed using various oxygen scavengers, e.g., sodium sulfite, hydrazine, and ascorbate, to determine whether the observed effect was that of dissolved oxygen removal or from any specific surface interaction with a particular oxygen scavenger (Figs. 1, S5, and S6). These oxygen scavengers were also sufficient to agglomerate the AgNPs to form the required nanoaggregates containing nano-gaps for SERS enhancement (Fig. S7). For blank aerobic experiments, sodium sulfate was used as an agglomerating agent.

Ultrahigh SERS sensitivity obtained by chemical oxygen removal

First, we observed that the SERS spectra of pATP and pNTP in aqueous samples increased dramatically after removal of the DO using sodium sulfite (Na_2SO_3, Fig. 1a and Fig. S5) based on the reaction $2Na_2SO_3 + O_2 \rightarrow 2Na_2SO_4$. The limit of detection (LOD)

for pATP reached the 10 zM level based on both its C-H bending (1135–1142 cm^{-1}, Figs. 1b and c) and C-S stretching (1070–1080 cm^{-1}, Fig. S8) vibrations (notably not all vibrational modes are equally sensitive and some vibrations became undetectable as the analyte concentration dropped, Fig. S6). In contrast, the LOD only reached 10 pM in an aerobic environment (Fig. 1d and Fig. S9). This corresponds to a 1 billion (10^9) times increase of the EF after oxygen removal. A similar EF increase was observed for the detection of other molecules, e.g., pNTP (Fig. S5 and S6) and four homopolymer oligoDNA sequences (Fig. S10 and Table S1). In addition, similar results were observed when the SERS substrates were spherical rather than prismatic Ag nanoparticles (Fig. S11), indicating the signal enhancement was unaffected by SERS substrate shape. To verify the effect of DO on the SERS signal intensity, we studied their quantitative correlation. The DO level was negatively proportional to the SERS signal intensity (Figs. 2a, 2b, and S12). We used two different methods to remove the DO in the aqueous solution, irreversible chemical oxygen scavenging using Na_2SO_3, hydrazine, or ascorbate, or physical removal using inert gas sparging. Both methods resulted in the same trend (Fig. 2a) with an inverse correlation between electrochemically determined DO concentration and the SERS LOD (Fig. S12). Hydrazine and ascorbate enabled the same zM level LOD for the model analyte pNTP as Na_2SO_3 did (Fig. S6).

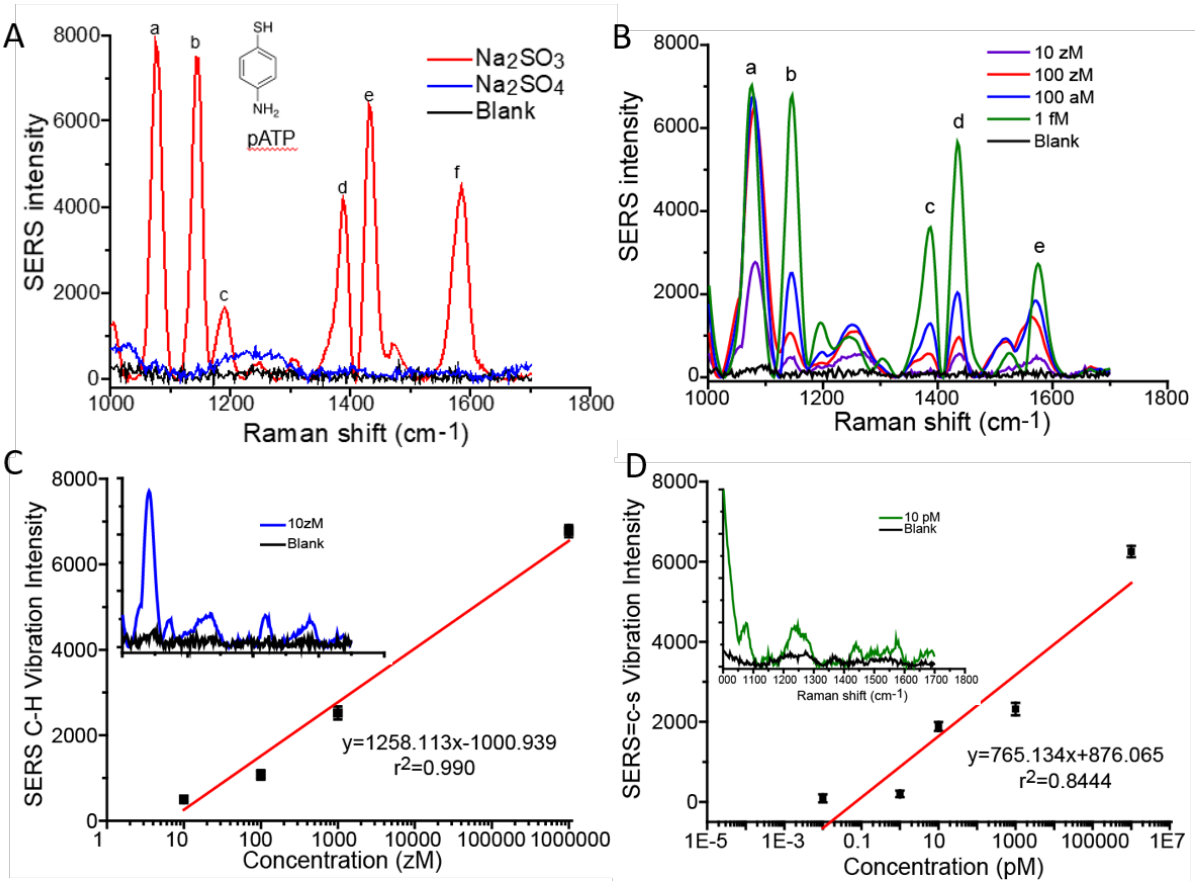

Figure 1. a) The SERS spectra of pATP in aqueous samples with and without removal of dissolved oxygen by using sodium sulfite (Na_2SO_3) as the oxygen scavenger, where sodium sulfate (Na_2SO_4) was used in control samples to maintain the ionic strength. The blank sample contained Na_2SO_3 but no pATP. c) The SERS spectra of samples (300 μL) containing various concentrations of pATP after oxygen removal. d) The intensity of the pATP C-H vibration as the function of pATP sample concentrations after oxygen removal. Inset: a comparison of the spectra between a 10 zM pATP solution and the Na_2SO_3 containing blank, showing that Na_2SO_3 does not generate any interfering signal. D) Without oxygen removal, the intensity of the pATP C-S vibration as the function of pATP sample concentrations. Inset: a comparison of the spectra between a 10 pM pATP solution and the Na_2SO_4 containing blank.

DO removal can decrease the formation of the Ag_2O layer on AgNP surfaces during SERS measurement in aqueous solution, which was confirmed by an undetectable amount of Ag^+ ions in the sample solution by an electrochemical measurement (Fig. S13);

in contrast, a significant amount of Ag^+ ions were detected in samples without DO removal, presumably because of oxidation of AgNP surfaces by DO, which becomes more significant under irradiation by the SERS laser (785 nm). Formation of the Ag_2O layer may affect the analyte adsorption and the charge transfer between the analyte molecules and the AgNPs, thus decreasing the chemical enhancement. Nevertheless, our results indicated the oxidation of Ag forming Ag_2O layer as a minor factor in comparison to the presence of DO in the sample. The hypothesis was validated by two experiments. First, we employed gold nanorods (AuNRs, Fig S14) as the SERS substrate, because AuNRs are chemically inert and resistant to oxidation, where cetyltrimethylammonium bromide (CTAB), a capping agent for AuNR synthesis to form rod-shaped templates that control the AuNR shape, was measured as the analyte. Similarly, DO removal by sodium sulfite enhanced the intensity of SERS signals for C_4N^+ and C-C vibrations drastically (Fig. 2c).[28] In the second experiment, the same signal enhancement was observed when using silica coated AgNPs as a substrate with an inert oxide layer, i.e., the above-mentioned SHINERS technique, where the LOD of the SHINERS detection decreased from the 500 nM to the 50 aM level, a sensitivity enhancement of 10^{10} times (Figs. 2d and S15). Although the sensitivity when using silica coated AgNPs is 10^4 times lower than that of using naked AgNPs as the substrate, DO, rather than the oxide layer on AgNP surfaces, appears to be the main factor that quenches the SERS signal (10^{10} times versus 10^4 times). Therefore, DO contributes more significantly to SERS attenuation than surface oxidation.

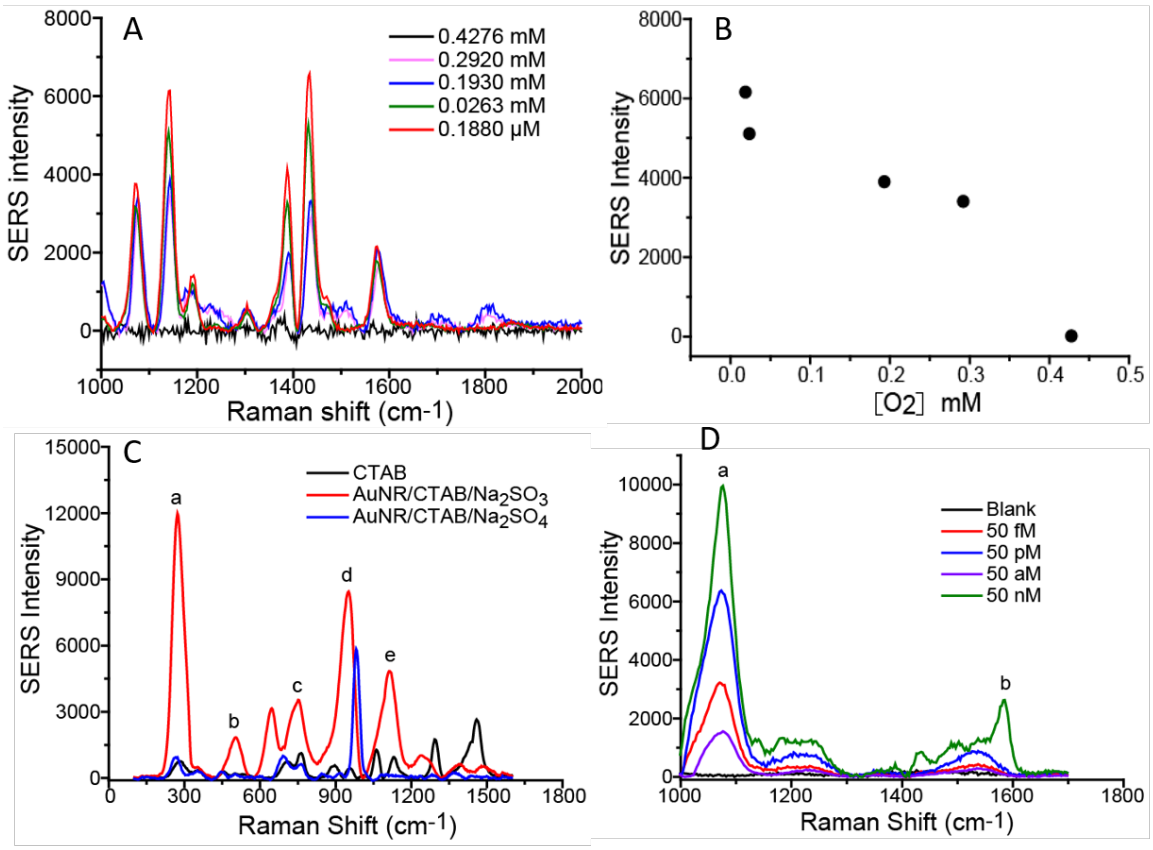

Figure 2. a) The SERS spectra of a fixed concentration of pATP in aqueous samples that contained different concentrations of dissolved oxygen by using various concentrations of Na_2SO_3 as the oxygen scavenger. b) The intensity of the pATP C-H vibration as the function of dissolved oxygen concentrations in the samples. c). The SERS spectra of cetyltrimethylammonium bromide (CTAB) on the surface of gold nanorods (AuNRs) with and without oxygen removal using Na_2SO_3. The peaks a, b, c, and d are vibrations of C_4N^+, whereas peak e is assigned as a C-C stretch. d) The SERS spectra of pATP on the surface of SiO_2-coated AgNPs after oxygen removal using Na_2SO_3. Peak a is assigned as a =C-S vibration and b is the C=C vibration in the benzene ring (see Fig. S17 for the confirmation of the pATP SERS spectrum). Note: When pATP concentrations were low and using SiO_2-coated AgNPs as substrates, only the =C-S and C=C vibrations were detectable.

This discovery brings out a challenge to the conventional understanding of the SERS measurement. Currently it is believed that the analyte molecule must be located in the field of view of the SERS detector that simultaneously excites the analyte molecule adsorbed on the AgNP surfaces and collects the light inelastically scattered by the analyte

using the same optical fiber bundle.[15,16] However, because the light path is so narrow (2.5 μm in diameter, Fig. S16), the probability of the analyte molecule existing within the view of the optical fiber was calculated to be 5.4 x 10^{-8}:1 based on the volume ratio of the light path to the sample (assuming that the light path is collimated instead of focussed) and assuming the probability of the analyte molecule is homogeneously distributed within the sample solution. Because the probability (5.4 x 10^{-8}:1) of the analyte molecule to be located within the light path is almost zero, it should not be detectable based on the conventional SERS theory. However, to our surprise, when we performed numerous independent analyses (n > 300 by different analysts on different days, even with AgNPs prepared in different batches) of analyte molecules at the zM level, we obtained consistently reproducible results. The measurements also include single blind studies where 20 samples were prepared by one researcher (A. J. C.) either containing 10 zM of pATP or a blank without pATP, which were then detected by an analyst (C. N.) who was unaware of the identity of the samples or the relative numbers of blanks and positive controls. The analyst never detected a SERS response in the blanks, but always observed the response in positive controls.

To rationalize our observation, we reason that, first, effective coupling of the SERS field can be achieved by oxygen removal, which is responsible for SERS signal enhancement. Second, such plasmonic coupling enables the propagation of the electromagnetic (EM) field, i.e., the photo energy, within the aqueous samples across long distances (up to the scale of centimetres and metres) with minimal energy loss, so that the plasmonic field generated upon excitation by the incident light can transport throughout the sample to

reach the AgNP with the adsorbed analyte molecule and also bring the Raman scattering signal of the molecules back to the optical fiber of the detector. Herein, because of the high electron affinity of molecular oxygen, either individual or clusters of DO molecules in the aqueous sample serve as electron traps that prevent the effective generation, coupling, propagation, and integration of the SERS field among individual AgNPs and AgNP aggregates. After DO removal, the aqueous solutions containing AgNP aggregates become optically conductive for SERS field transport, similar to an optical fiber.

The first hypothesis was verified by computing the plasmonic EM field surrounding an aggregate that contains one spherical AgNP between two nano-prisms in aqueous solution induced by incident light (Fig. 3). The distribution of the EM field (Fig. 3a) indicates strong plasmonic coupling is present among the AgNPs and becomes intensified within the nano-gaps, which are hot-spots. However, the presence of DO molecules suspended within the nano-gaps (Fig. 3c) or adsorbed onto the AgNP surface (Fig. S17) results in charge redistribution (Figs. 3d and S17d), and thus strong quenching of the plasmonic EM field on left half of the aggregate that prevents the EM coupling. We further calculated the distribution of the EM field (Fig. S18) around a AgNP conjugate with a 3 nm thick Ag_2O layer caused by surface oxidation; we still observed a strong plasmonic EM field around the AgNP aggregate surface (Fig S18b), although the coupling of the EM field is not so strong in comparison to that around the AgNP conjugate without a Ag_2O layer (Fig. 3a); this result indicates that the presence of a Ag_2O layer may compromise the SERS performance,[29] but is insufficient to make the SERS coupling ineffective,[29] which is consistent with our experimental results and those reported previously.[26,29]

However, the presence of DO seriously quenches the plasmonic EM field on the right half and prevents its coupling (Fig. S18c–h). Taken together, the computational modeling of the plasmonic EM field around AgNPs in the presence or absence of DO supports the hypothesis that DO quenches the SERS field, resulting in sensitivity loss; in contrast, in the absence of DO, the plasmonic EM field can propagate through the sample solution via neighboring AgNPs and their aggregates as a result of the effect of plasmonic coupling.

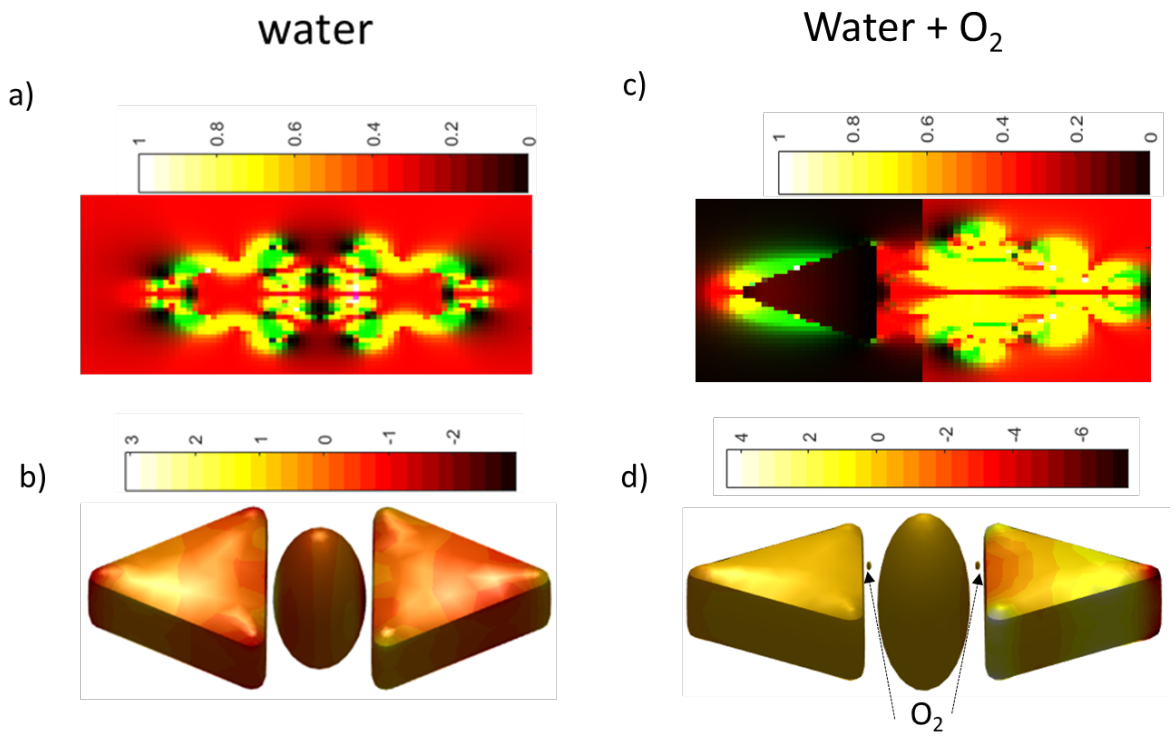

Figure 3. a) The electromagnetic field distribution surrounding an aggregate containing one spherical AgNP between two nanoprisms in aqueous solution without dissolved oxygen and b) its corresponding charge distribution and c) the electromagnetic field distribution with two oxygen molecules suspended in the nanogaps between the nanoprisms and the spherical AgNP and d) its corresponding charge distribution.

To test the second hypothesis, we studied the propagation of the SERS signals in aqueous solution. First, we tested the photocurrent induced by the laser irradiation on AgNPs that are suspended in the electrolyte solution but not physically attached to the gold electrode (Scheme S1 and Fig. 4a). The results showed that, upon DO removal with Na_2SO_3, the photocurrent is significantly enhanced in comparison with the control, where the same amount of Na_2SO_4 was added as the electrolyte (Fig. 4a). Second, we detected the analyte adsorbed on a Ag substrate far away from the light path of the laser beam. In this work, we coated the end of a 10-cm quartz NMR tube with a small silver mirror (5 mm in length) to adsorb pATP molecules through the thiol group. After extensive rinsing with ethanol and nanopure water to remove any non-specifically bound pATP in the tube (30 rinses with each, always rinsing out from the tube opening with the silver mirror coating where the pATP was bound), the tube was filled with AgNP solution in nanopure water without any analyte. The position of the laser with respect to the silver mirror coating was tuned to study the SERS signal intensity as the function of the distance between the laser focal point and the silver mirror with adsorbed analyte molecules (Scheme S2 and Figs. 4b and S19). Surprisingly, we found that without DO (using Na_2SO_3 for DO removal), the SERS signal did not attenuate over 10 cm. The SERS signal was still strong even after the distance was increased to 1 meter where we coupled the NMR tube to a 1 m PEEK capillary tubing (Figs. 4c and S20), demonstrating its capability of remote sensing of molecules. However, when we used silica coated AgNPs as the substrate (Scheme S2), the intensity of the SERS signal decreased rapidly over distances (Fig. 4d); nevertheless, DO removal is critical in affecting the propagation of the plasmonic EM field.

Furthermore, rapid screening of multiple samples within 2 minutes could be achieved by adsorbing analytes to a silver-mirror-coated 96-well microtitre plate by filling the wells with deoxygenated and agglomerated AgNP solutions and dipping a glass capillary tube containing the same solution and irradiated with the Raman laser sequentially into each well (Fig. S21). Analyte signals are observed only when the capillary is inserted into each well. A subsequent single blind test of the remote sensing was performed by creating 20 samples, each containing a final concentration of either 0 or 1 μM of pNTP pre-adsorbed onto AgNPs (3.5 nM) that were agglomerated using saturated Na_2SO_3 solution (final volume 40 μL), into which a glass capillary tube pre-filled with deoxygenated and agglomerated AgNPs was dipped with the distal end (6 cm) in the focus of the Raman laser. The number and identity of the positive (n=9) and negative (n=11) controls were prepared and randomly selected by one investigator (A. J. C.) (see detailed sample preparation in the SI) and were subsequently detected by the analyst (C. N.), who was blinded and measured and processed the obtained spectra and was able to 100% unambiguously identify all the positive and negative controls. The accurate remote sensing experiments demonstrated that the aqueous AgNP suspension serves as an optical fiber that facilitates SERS signal transport.

Previous understanding of SERS is based on signal amplification with individual nanostructures or the plasmonic field coupling of adjacent nanoparticles, i.e., nano-gaps, because DO serves as an electron sink in the solution thus preventing the plasmonic EM field propagation within and among the aggregate of AgNPs. The “hot spot” theory is sufficient to interpret all the experimental observations, of which the signal amplification

of SERS is based on “localized surface-plasmon resonance (LSPR)”, which is a discrete EM field around individual or small clusters of nanoparticles.[11] However, for the first time, our work demonstrates that large-scale plasmonic field coupling (integrated surface-plasmon resonance (ISPR)) is possible upon DO removal. Such an integrated field endows the possibility of effective transport of the SERS signal of one single molecule that is adsorbed on any individual nanoparticle surface throughout the whole sample solution. Thus, every nanoparticle is SERS active and can facilitate generating SERS signals when there are analyte molecules adsorbed on its surface, similar to a “hotspot”, or transport the SERS signal,[30] breaking the boundary of the EM communication within and between NP aggregates, resulting in real single molecule detection.[31]

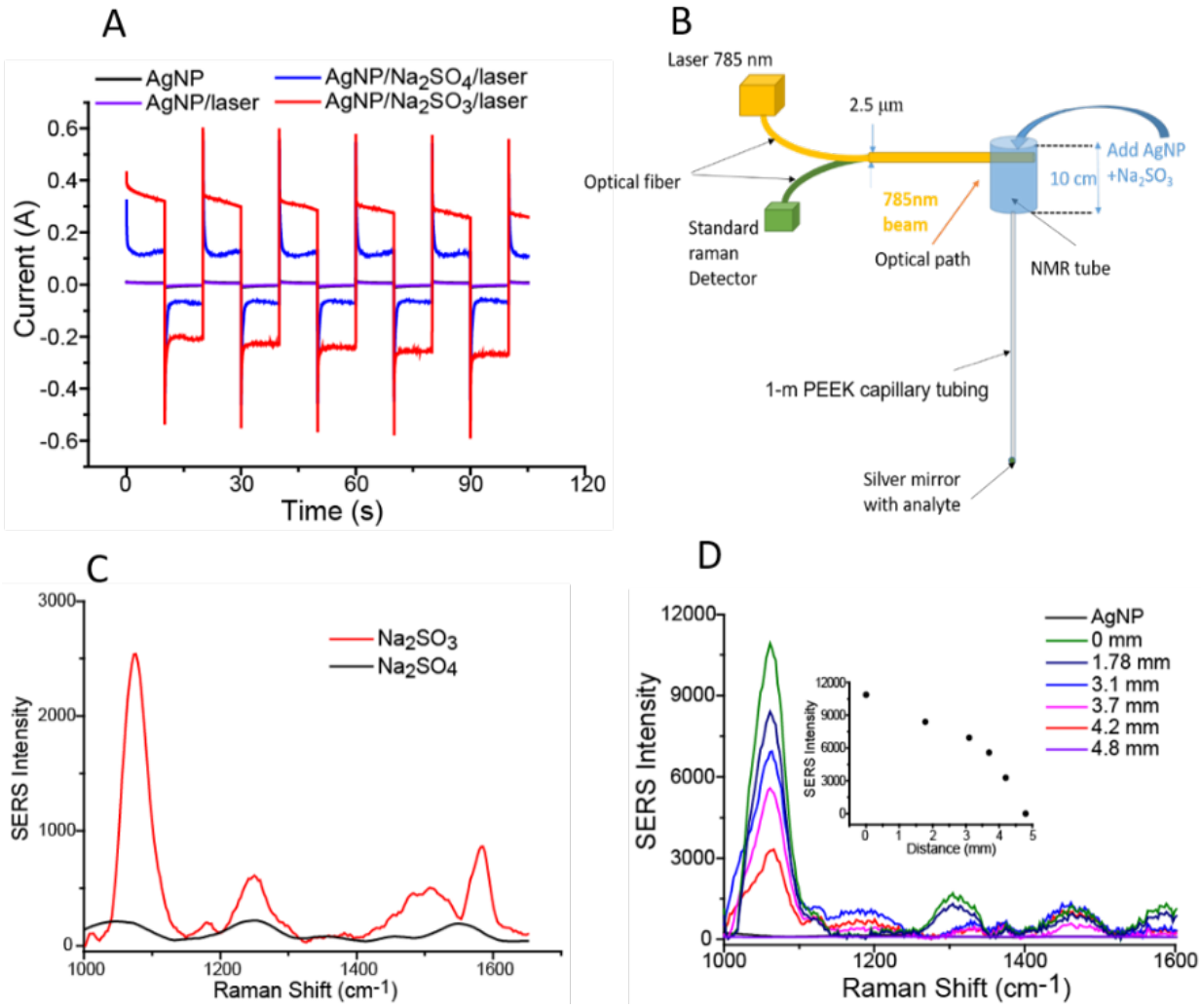

Figure 4. a) The photocurrent generated on the electrode surface within the plasmonic field of AgNPs induced by the irradiation of a NIR laser (wavelength: 785 nm). b) The experimental setup for the remote sensing SERS. c) The remote SERS spectra of the analyte adsorbed on the silver mirror at the end of the 1 m tubing. d) The SERS signal intensity as a function of the distance between the analyte (adsorbed on the silver mirror) and the laser. The inset shows the intensity of =C-S vibration (Raman shift: 1050 cm^{-1}) as the function of the distance from the laser to the analytes.

One striking advantage is that the detection time is not determined by the diffusion of the analyte molecules in sample solutions (particularly because they are surface bound to slowly diffusing nanoparticle aggregates), but the transport of the plasmonic field

throughout the solution, which is much faster than molecular diffusion. In our remote SERS detection (Fig. 4c), where the analyte molecules were immobilized on the silver mirror at the end of the 1 m tubing, and thus unable to migrate in solution, the SERS signal of the analyte was obtained immediately upon irradiation. Such ultra-fast response gives the SERS detection high temporal resolution in addition to its high sensitivity, allowing the monitoring of fast chemical events, e.g., to study chemical reactions or to detect short-lived species, such as reactive oxygen species, at a single molecule level.

Meanwhile, our work demonstrates a cost-effective approach to develop ultrasensitive SERS instruments based on a regular Raman spectrometer, without using expensive SERS detectors. This greatly reduces the capital expense of performing SERS experiments and will facilitate this research globally, but particularly in developing countries and resource-limited areas.

We believe the unprecedented detection sensitivity, fast response time, and the remote sensing capability may generate many applications in medical diagnosis, environmental monitoring, and national security.

Acknowledgements

This work was supported by the Canada Research Chairs program, New Frontiers in Research Fund - Exploration (NFRFE-2018-01005), Nova Scotia Lands Boat Harbour Remediation Program, Cape Breton University RISE program, NSERC Discovery Grants Program, the Atlantic Canada Opportunities Agency AIF program, and Beatrice Hunter

Cancer Research Institute. The authors gratefully acknowledge helpful discussions with Dr. Christa Brosseau of Saint Mary's University, Halifax, Nova Scotia, Canada.

Author contributions

C. N., A.J.C., and X.Z. conceived the idea and designed the research; C. N., A.J.C., D.O., D. Y., N. Y., D. R., C. B., C. B., and C. N. performed experimental research; A.J.C., Y.C., K.O, S.L.M., and X.Z. wrote the manuscript.

Completing Interest Statement

The authors declare no competing interests.

References

References

1 Sharma, B., Frontiera, R. R., Henry, A.-I., Ringe, E. & Van Duyne, R. P. SERS: Materials, applications, and the future. *Materials Today* **15**, 16-25, doi.org/10.1016/S1369-7021(12)70017-2 (2012).

2 Sharma, B. Bisboronic acids for selective, physiologically relevant direct glucose sensing with surface-enhanced Raman spectroscopy. *J. Am. Chem. Soc.* **138**, 13952-13959 (2016).

3 Powell, J. A., Venkatakrishnan, K. & Tan, B. Programmable SERS active substrates for chemical and biosensing applications using amorphous/crystalline hybrid silicon nanomaterial. *Scientific Reports* **6**, 19663, doi:10.1038/srep19663 (2016).

4 Sun, F. *et al.* Hierarchical zwitterionic modification of a SERS substrate enables real-time drug monitoring in blood plasma. *Nature Communications* **7**, 13437, doi:10.1038/ncomms13437 (2016).

5 Dyakonov, P. *et al.* Carbon nanowalls as a platform for biological SERS studies. *Scientific Reports* **7**, 13352, doi:10.1038/s41598-017-13087-8 (2017).
6 Halvorson, R. A. & Vikesland, P. J. Surface-Enhanced Raman Spectroscopy (SERS) for Environmental Analyses. *Environmental Science & Technology* **44**, 7749-7755, doi:10.1021/es101228z (2010).
7 Fleischmann, M., Hendra, P. J. & McQuillan, A. J. Raman spectra of pyridine adsorbed at a silver electrode. *Chem. Phys. Lett.* **26**, 163-166 (1974).
8 Jeanmaire, D. L. & Van Duyne, R. P. Surface Raman spectroelectrochemistry: part I. Heterocyclic, aromatic, and aliphatic amines adsorbed on the anodized silver electrode. *J. Electroanal. Chem. Interfacial Electrochem.* **84**, 1-20 (1977).
9 Nie, S. & Emory, S. R. Probing Single Molecules and Single Nanoparticles by Surface-Enhanced Raman Scattering. *Science* **275**, 1102-1106, doi:10.1126/science.275.5303.1102 (1997).
10 Kneipp, K. *et al.* Single Molecule Detection Using Surface-Enhanced Raman Scattering (SERS). *Physical Review Letters* **78**, 1667-1670, doi:10.1103/PhysRevLett.78.1667 (1997).
11 Ding, S.-Y. *et al.* Nanostructure-based plasmon-enhanced Raman spectroscopy for surface analysis of materials. *Nature Reviews Materials* **1**, 16021, doi:10.1038/natrevmats.2016.21 (2016).
12 Ahmed, A. & Gordon, R. Directivity Enhanced Raman Spectroscopy Using Nanoantennas. *Nano Letters* **11**, 1800-1803, doi:10.1021/nl200461w (2011).
13 Radziuk, D. & Moehwald, H. Prospects for plasmonic hot spots in single molecule SERS towards the chemical imaging of live cells. *Physical Chemistry Chemical Physics* **17**, 21072-21093, doi:10.1039/C4CP04946B (2015).
14 Dong, L. *et al.* Nanogapped Au Antennas for Ultrasensitive Surface-Enhanced Infrared Absorption Spectroscopy. *Nano Letters* **17**, 5768-5774, doi:10.1021/acs.nanolett.7b02736 (2017).
15 Ahmed, A. & Gordon, R. Single Molecule Directivity Enhanced Raman Scattering using Nanoantennas. *Nano Letters* **12**, 2625-2630, doi:10.1021/nl301029e (2012).
16 Yilmaz, M. *et al.* Nanostructured organic semiconductor films for molecular detection with surface-enhanced Raman spectroscopy. *Nature Materials* **16**, 918, doi:10.1038/nmat4957 (2017).
17 Yang, S., Dai, X., Stogin, B. B. & Wong, T. S. Ultrasensitive surface-enhanced Raman scattering detection in common fluids. *Proc. Natl Acad. Sci. Usa* **113**, 268-273 (2016).
18 De Angelis, F. *et al.* Breaking the diffusion limit with super-hydrophobic delivery of molecules to plasmonic nanofocusing SERS structures. *Nature Photonics* **5**, 682, doi:10.1038/nphoton.2011.222 (2011).
19 Christopher, P., Xin, H. & Linic, S. Visible-light-enhanced catalytic oxidation reactions on plasmonic silver nanostructures. *Nature Chemistry* **3**, 467, doi:10.1038/nchem.1032 (2011).
20 Li, J. F. *et al.* Surface analysis using shell-isolated nanoparticle-enhanced Raman spectroscopy. *Nature Protocols* **8**, 52, doi:10.1038/nprot.2012.141 (2012).
21 Erol, M. *et al.* SERS Not To Be Taken for Granted in the Presence of Oxygen. *Journal of the American Chemical Society* **131**, 7480-7481, doi:10.1021/ja807458x (2009).

22 Han, Y. *et al.* Effect of Oxidation on Surface-Enhanced Raman Scattering Activity of Silver Nanoparticles: A Quantitative Correlation. *Analytical Chemistry* **83**, 5873-5880, doi:10.1021/ac2005839 (2011).
23 Li, J.-F., Zhang, Y.-J., Ding, S.-Y., Panneerselvam, R. & Tian, Z.-Q. Core–Shell Nanoparticle-Enhanced Raman Spectroscopy. *Chemical Reviews* **117**, 5002-5069, doi:10.1021/acs.chemrev.6b00596 (2017).
24 Michieli, N. *et al.* Oxidation effects on the SERS response of silver nanoprism arrays. *RSC Advances* **7**, 369-378, doi:10.1039/C6RA26307K (2017).
25 Matikainen, A. *et al.* Atmospheric oxidation and carbon contamination of silver and its effect on surface-enhanced Raman spectroscopy (SERS). *Scientific Reports* **6**, 37192, doi:10.1038/srep37192 (2016).
26 Li, J. F. *et al.* Shell-isolated nanoparticle-enhanced Raman spectroscopy. *Nature* **464**, 392, doi:10.1038/nature08907 (2010).
27 Zhang, Q., Li, N., Goebl, J., Lu, Z. & Yin, Y. A Systematic Study of the Synthesis of Silver Nanoplates: Is Citrate a "Magic" Reagent? *Journal of the American Chemical Society* **133**, 18931-18939, doi:10.1021/ja2080345 (2011).
28 Dendramis, A. L., Schwinn, E. W. & Sperline, R. P. A surface-enhanced Raman scattering study of CTAB adsorption on copper. *Surface Science* **134**, 675-688, doi:1016/0039-6028(83)90065-1 (1983).
29 Bakker, R. M. *et al.* Magnetic and Electric Hotspots with Silicon Nanodimers. *Nano Letters* **15**, 2137-2142, doi:10.1021/acs.nanolett.5b00128 (2015).
30 Shalabney, A. *et al.* Enhanced Raman Scattering from Vibro-Polariton Hybrid States. *Angewandte Chemie International Edition* **54**, 7971-7975, doi:10.1002/anie.201502979 (2015).
31 Maier, S. A. *et al.* Local detection of electromagnetic energy transport below the diffraction limit in metal nanoparticle plasmon waveguides. *Nature Materials* **2**, 229-232, doi:10.1038/nmat852 (2003).

Supplementary Information for

Effective plasmonic coupling and propagation facilitates ultrasensitive and remote sensing using Surface Enhanced Raman Spectroscopy

Collins Nganou,[a] Andrew J. Carrier,[a] Dongchang Yang,[a] Yongli Chen,[b] Naizhen Yu,[a] Doug Richards,[a] Craig Bennett,[c] Ken Oakes,[d] Stephanie L. MacQuarrie,[a] and Xu Zhang*[a]

[a]Department of Chemistry, Cape Breton University, Sydney, Nova Scotia, B1P 6L2, Canada

[b]Postdoctoral Innovation Practice Base, Shenzhen Polytechnic, Shenzhen, 518055, China

[c]Department of Physics, Acadia University, Wolfville, Nova Scotia, B4P 2R6, Canada

[d]Department of Biology, Cape Breton University, Sydney, Nova Scotia, B1P 6L2, Canada

*Corresponding Author. E-mail: Xu_Zhang@cbu.ca

Detailed Experimental and Discussion Sections

Materials

All reagents were commercially available and used without further purification. Silver nitrate ($AgNO_3$, 99.9%), sodium borohydride ($NaBH_4$, 99%), trisodium citrate (99%), 4-aminothiophenol (pATP, 99%), 4-nitrothiophenol (pNTP, 99%), tetraethylorthosilicate (TEOS, 98%), sodium hydroxide (99%), sodium sulfate (99%), sodium sulfite (99%), and ammonium hydroxide (30%) were purchased from Sigma-Aldrich (Oakville, ON, Canada). Anhydrous ethanol (EtOH) and hydrogen peroxide (H_2O_2, 30 wt%) were purchased from VWR (Mississauga, ON, Canada). Single stranded thiolated DNA 5-mers, i.e., 5A, 5C, 5G, and 5T, were purchased from Eurofins MWG Operon (Huntsville, AL, USA). Nanopure water (18 MΩ cm) was obtained from a Barnstead Nanopure system (Thermo Fisher Scientific).

Silver Nanoplate Synthesis

Silver nanoplates (AgNP) were prepared using the method reported by Zhang et al.,[31] which is briefly described here. $AgNO_3$ (50 µL, 0.05 M), trisodium citrate (0.5 mL, 75 mM), EtOH (0.1 mL, 17.5 mM), and H_2O_2 (60 μL, 30 wt%) were mixed in 25 mL of nanopure water and stirred at 1200 rpm. To this was added $NaBH_4$ (200 μL, 100 mM) resulting in a

color change from yellow to light blue. The resultant AgNPs had an absorbance maximum at 590 nm, and TEM imaging revealed triangular nanoplates with an average diameter of 17±2 nm. As prepared the AgNPs had a concentration of 0.3 nM that was concentrated to 7 nM by centrifugation at 12 000 rpm for 20 min. TEM images of the prepared nanoplates are given in Fig. S1.

SiO_2-coated AgNPs

Equal volumes of AgNP (7 nM) and TEOS (1 μM) were mixed in EtOH in a 1.5 mL polypropylene microcentrifuge tube before ultrasonication for 10 min. No aggregation was observed after centrifugation at 12 500 rpm for 20 min. To agglomerate these particles for SERS measurements the solution pH was adjusted to 4 before adding Na_2SO_4 or Na_2SO_3.

Electrochemical Measurements

Amperometry experiments were performed using a bipotentiostat CS2350 (Wuhan Corrtest Instruments Corp., Ltd., Wuhan, China). Screen-printed gold honeycomb working and counter electrodes were used with an external 1M Ag/AgCl reference electrode (Pine Research Instrumentation, Durham, NC, USA). The honeycomb electrodes have 19 holes separated by 0.75 mm. Each hole has a diameter of 0.50 mm and a depth of 1.5 mm, which allows the AgNPs to pass through the working electrode.

The solution was stirred at 1200 rpm using a 2 mm magnetic stir bar. For all the potential range measurements the initial potential was 0 V. The low and high potentials were -0.9, -1, -1.7, and +0.9, +1, +1.7 V, respectively.

The current enhancement was independent of the above-applied voltage. No contribution of electrode instability was observed. The pulse width was 10 s at a frequency of 10 Hz. A quartz cuvette was used as the sample holder (with no background interference observed, relevant blanks given in Figs. S22–S24). The sample was irradiated with a 785 nm laser outside of the electrode area (see Scheme S1 in Page S35).

Surface Enhanced Raman Spectroscopy

To evaluate the detection sensitivity for different analytes adsorbed on the AgNPs, SERS signals were measured in a 5 x 100 mm quartz NMR tube (0.5 mm quartz thickness). Samples were excited using a solid-state Nd-YAG laser (785 nm, line width <3.2 cm^{-1}, 500 mW). The laser stability was ±5% with a resolution of 5–8 cm^{-1}. A 785 nm fiberoptic laser probe was connected to the laser source with an output power of 450 mW and a beam diameter 2.5 µm. The power at the sample (~5 mW, shown in Fig. S25) was recorded with a thorlabs PM100 optical power meter. Backscattered (180º) light was collected by a standard Sunshine TG-Raman fiber spectrometer (Changchun New Industries Optoelectronics Tech. Co., Ltd., Changchun, China). The SERS spectra were collected above 1000 cm^{-1} because of the strong spectra interference of the capping

molecules, i.e., citrate and ethanol. However, sample spectra between 200–1650 cm^{-1} are presented to support our claims (see Figs. S3, S6, S14, S15, and S19–21).

Sample Preparation and Oxygen Removal

Different concentrations of pATP from 40 μM to 40 zM were prepared in EtOH by serial dilution, and pATP and AgNP solutions were mixed to obtain the target pATP concentration, e.g., 75 μL of pATP and AgNP solutions and 150 μL of nanopure water. Each concentration was prepared in 3 replicates to obtain a standard deviation. To each pATP+AgNP solution (300 μL) was added 10 mg of either Na_2SO_3 or Na_2SO_4 to yield solutions with identical ionic strength and either the removal or retention of dissolved oxygen. The samples were analyzed as described above.

Remote Sensing

To determine the extent of plasmonic coupling within and between the nanoparticle aggregates, we devised two experiments. We sought to isolate the analyte molecules from the incident light source and field of view of the detector by adsorbing them on a silver mirror surface and thoroughly removing any unadsorbed or loosely bound analytes through extensive rinsing (Scheme S2). This was achieved either using a 10 cm long quartz NMR tube or a 1 m long PEEK capillary tube coupled to a short section of quartz NMR tubing.

First, to prepare the silver mirror surface at the end of the tubing, a solution of Tollen's reagent was prepared from 0.1 M of $AgNO_3$, which was first precipitated by the addition of dilute NaOH to form Ag_2O. The obtained Ag_2O was re-dissolved by the dropwise addition of concentrated aqueous NH_3 to form the $Ag(NH_3)_2$ complex. The Tollen's reagent solution was added either to a quartz NMR tube or to the surface of PEEK tubing in a polypropylene microcentrifuge tube to cover half of the desired surface (~ 5 mm) that should be silver-coated. Then, an equal volume of 0.1 M of glucose was added, and the mirror was allowed to develop. After the surface was silver-coated, it was rinsed ~30 times each with nanopure water and EtOH to remove any excess reagents or other adsorbed materials before drying at ambient temperature. Note that the adhesion of silver on the polymer surfaces is weak and should be treated with care as it can be rubbed off easily. Afterwards, 100 nM of pATP was added to cover the silver mirror surface. The NMR tube and the PEEK tubing were then rinsed 30 times each with EtOH and nanopure water to remove any unbound pATP from the silver mirror surface (for the PEEK tubing the rinsing was performed from the end opposite the silver mirror to prevent analyte migration into the tubing). To detect the analyte adsorbed at the distal end of a glass NMR tube or PEEK tubing, the thoroughly rinsed apparatus was filled with a AgNP solution that had been agglomerated and deoxygenated immediately prior through the addition of excess Na_2SO_3. The fiberoptic bundle connected to the incident laser light source and detector was aligned on the end of the cuvette or tubing opposite to the adsorbed analyte and the Raman spectrum was recorded. Analytes were detected when the AgNPs were

agglomerated and deoxygenated with Na_2SO_3, but not when they were only agglomerated with Na_2SO_4.

Single Blind Remote Sensing from Nanoparticle Aggregates

Samples for remote sensing were prepared for blind testing by making stock solutions, with either 0 or 2 μM of pNTP and 3.5 nM of AgNPs in 50 vol% ethanol (400 μL). The solutions were sonicated for 30 min to ensure the pNTP and AgNPs were well mixed and the pNTP had adsorbed onto the NP surfaces. To remove any residual unadsorbed pNTP, which could diffuse through solution, the samples were centrifuged for 30 min at 12700 rpm to precipitate the NPs and all but 20 μL of solution was removed (so as to not disturb the precipitated NPs). The samples were diluted to 1500 μL with ethanol and sonicated for an additional 30 min. This process was repeated for a total of two washings (reducing the maximum possible free pNTP to ~356 pM) before a final centrifugation, solvent removal (to 20 μL) and resuspension in 50 wt% ethanol with a final maximum possible free pNTP concentration of ~18 pM. The 20 μL of the samples were randomly assigned to 20 microcentrifuge tubes and diluted with 20 μL of water (for a final maximum free pNTP concentration of ~9 pM if none of the pNTP was adsorbed, estimated positive control AgNP-adsorbed concentration 1 μM). The number and identity of the positive and negative controls were masked from the analyst (C. N.), who prior to measurement simultaneously agglomerated and deoxygenated the samples through the addition of Na_2SO_3 powder. Glass capillary tubes that were pre-filled with solutions of agglomerated

and deoxygenated AgNP solutions were aligned with the Raman laser and dipped into the agglomerated sample solutions (6 cm from the incident light) and the Raman spectra were recorded and were assigned as positive and negative controls by the analyst who was blinded. The sample assignments were compared to their identities and all samples (positive controls n=9, negative controls n=11) were correctly identified.

Theoretical Interpretation

To understand how Ag_2O and O_2 influence the SERS signal response, we modelled the electromagnetic field (E-Field) enhancement of the surface plasmon nanocavity (Fig. 2c), using the boundary element method (BEM) approach.[32-34] The surface integral depends on the scalar and vector potentials of the interfacial charge and current, which are related to the frequency-dependent local dielectric function.[34] The surface charges are hypothesized to be located at the center of individual infinitesimal triangles (with index j).[32,35]

The E-field is expressed as scalar and vector potentials, φ (electric scalar potential) and A (magnetic vector potential), respectively:

$$E = ikA - \nabla\varphi \quad (2)$$

After applying the boundary condition, the electric displacement (D) at the interface surface (s) of two media, 1 and 2, are proposed to be (n_s normal vector and ε_a the dielectric function of the medium a):[34]

$$D^e = n_s \,.\, [\varepsilon_1(ikA_1^e - \nabla_s\varphi_1^e) - \varepsilon_2(ikA_2^e - \nabla_s\varphi_2^e) \quad (3)$$

We adopted the introduction of the compact matrix notation for the convolutions in space. The electric displacement in a system without oxygen or an oxide layer will be the sum of electric displacement over each interface of each AgNP, yielding:

$$D^e = n_{Ag-water} \,.\, [\varepsilon_{Ag}(ikA_1^e - \nabla_s\varphi_1^e) - \varepsilon_{water}(ikA_2^e - \nabla_s\varphi_2^e)] \quad (4)$$

In the equation Ag denotes the AgNPs, Ag_xO represents the oxide layer, and O_2 is molecular oxygen. In a system with an oxide layer, the electric displacement of each AgNP will be:

$$D^e = n_{Ag-Ag_xO} \,.\, \left[\varepsilon_{Ag}\left(ikA_{Ag}^e - \nabla_s\varphi_{Ag}^e\right) - \varepsilon_{Ag_xO}\left(ikA_{Ag_xO}^e - \nabla_s\varphi_{Ag_xO}^e\right)\right] +$$
$$n_{Ag_xO-water} \,.\, \left[\varepsilon_{Ag_xO}\left(ikA_{Ag_xO}^e - \nabla_s\varphi_{Ag_xO}^e\right) - \varepsilon_{water}(ikA_{water}^e - \nabla_s\varphi_{water}^e)\right] \quad (5)$$

When oxygen is present in the medium, each AgNP will have the following electric displacement:

$$D^e = n_{Ag-Ag_xO} \cdot \left[\varepsilon_{Ag}(ikA_1^e - \nabla_s\varphi_1^e) - \varepsilon_{Ag_xO}(ikA_2^e - \nabla_s\varphi_2^e)\right] + n_{Ag_xO-O_2} \cdot \left[\varepsilon_{Ag_xO}\left(ikA_{Ag_xO}^e - \nabla_s\varphi_{Ag_xO}^e\right) - \varepsilon_{O_2}\left(ikA_{O_2}^e - \nabla_s\varphi_{O_2}^e\right)\right] + n_{O_2-water} \cdot \left[\varepsilon_{O_2}\left(ikA_{O_2}^e - \nabla_s\varphi_{O_2}^e\right) - \varepsilon_{water}(ikA_{water}^e - \nabla_s\varphi_{water}^e)\right] \quad (6)$$

Detailed elaboration of the BEM method and it application for NP surface plasmons can be found in the literature.[33,34,36,37] The dielectric coefficients for AgNPs,[38] Ag_xO,[39] oxygen,[40] and water[40] can also be found in the literature.

The results of the modeling were shown in Figs. 3, S17, and S18.

Supplementary Figures

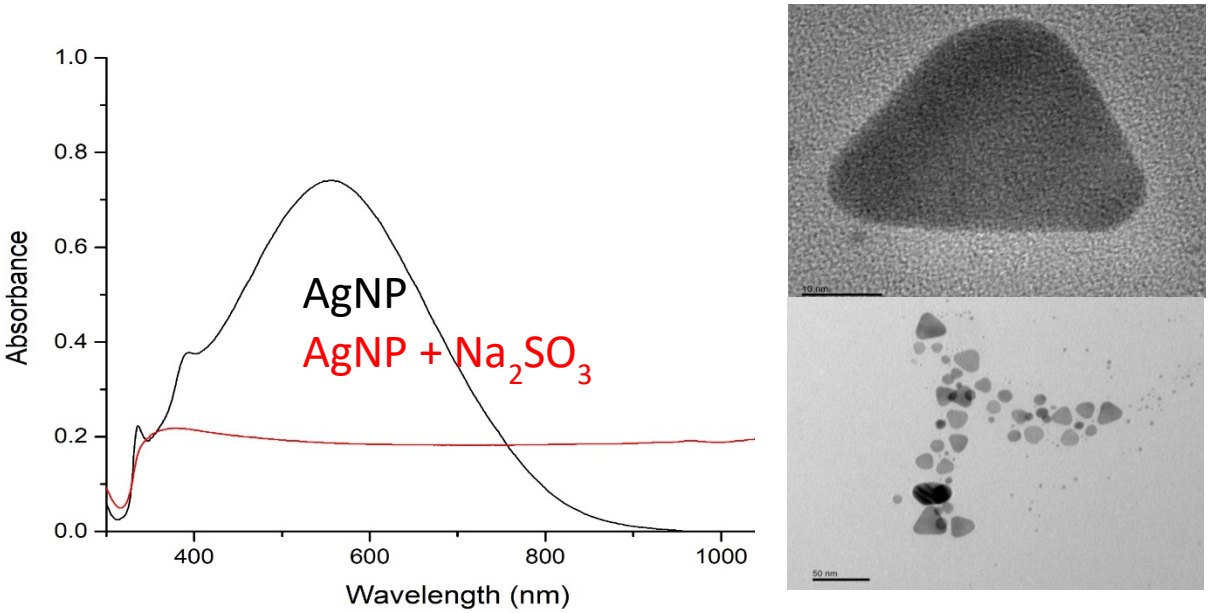

Figure S1. (left) UV-Vis spectrum of the dissolved and agglomerated AgNPs and (right) corresponding TEM images.

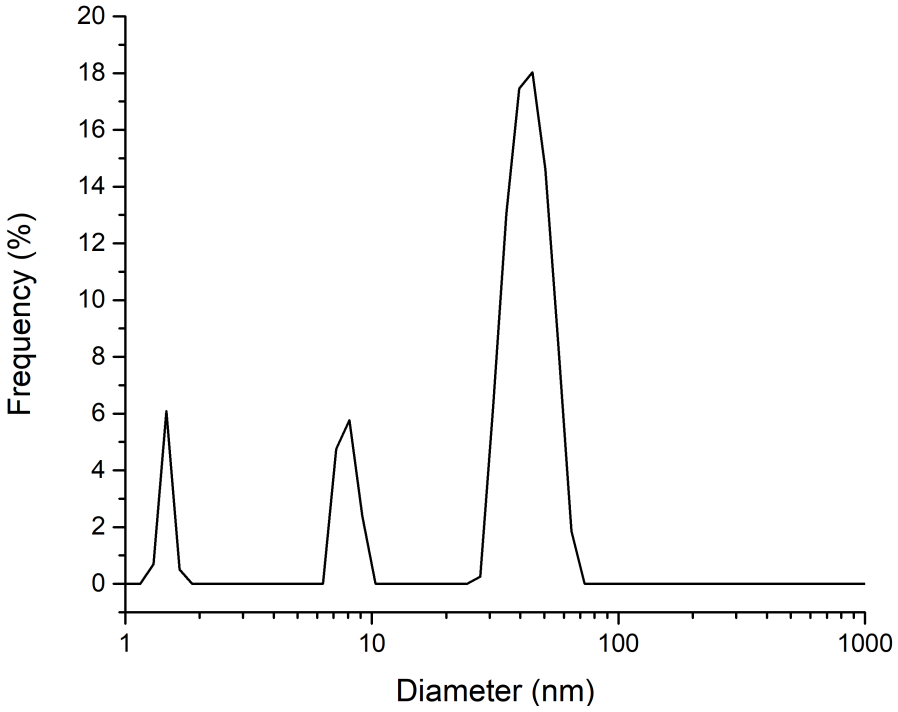

Figure S2. AgNP hydrodynamic size distribution as determined through dynamic light scattering.

Figure S3. The Raman spectra of pNTP and pATP.

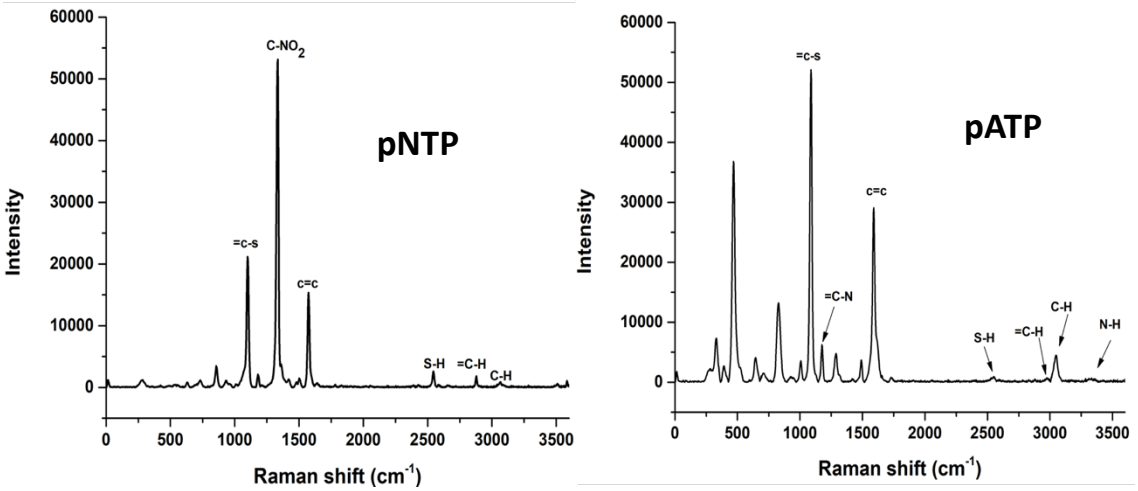

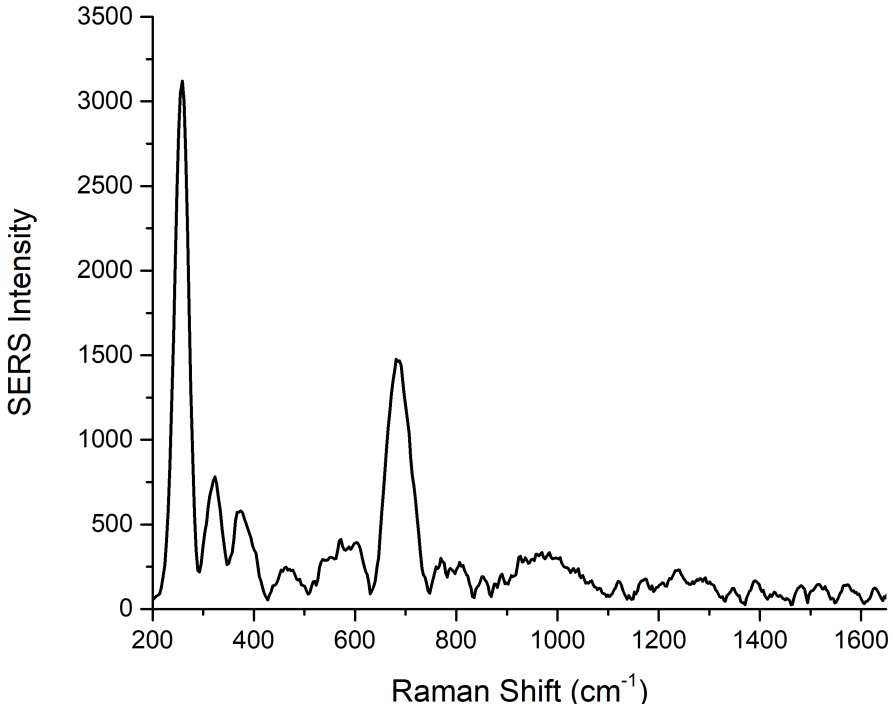

Figure S4. SERS spectrum of blank AgNPs showing strong signals from citrate and ethanol capping agents <1000 cm^{-1}.

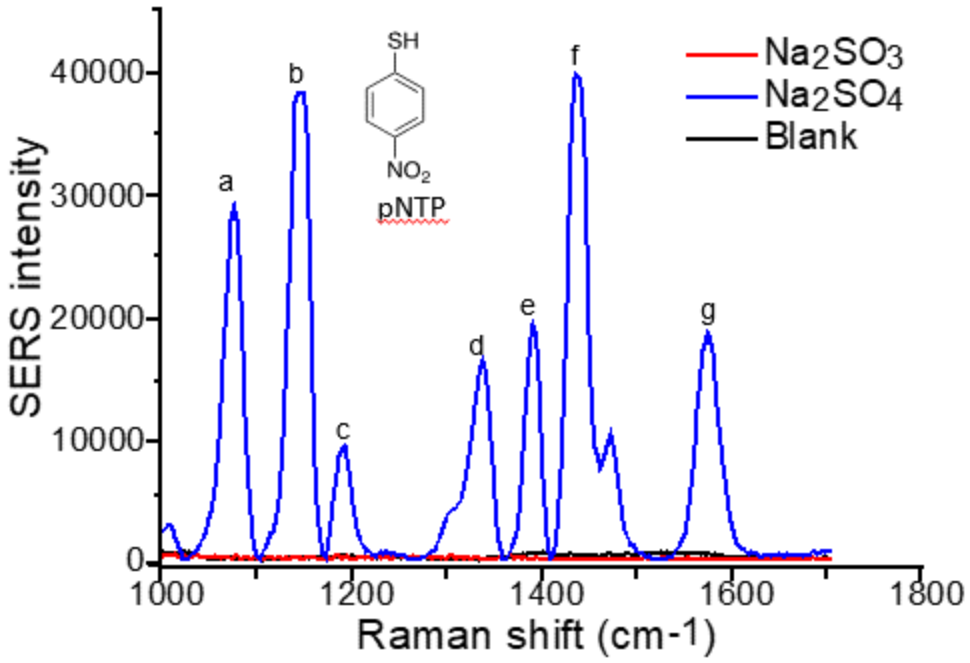

Figure S5. The SERS spectra of pNTP before and after removal of dissolved oxygen using Na_2SO_3. Na_2SO_4 was used in the control sample. The blank sample contained Na_2SO_3.

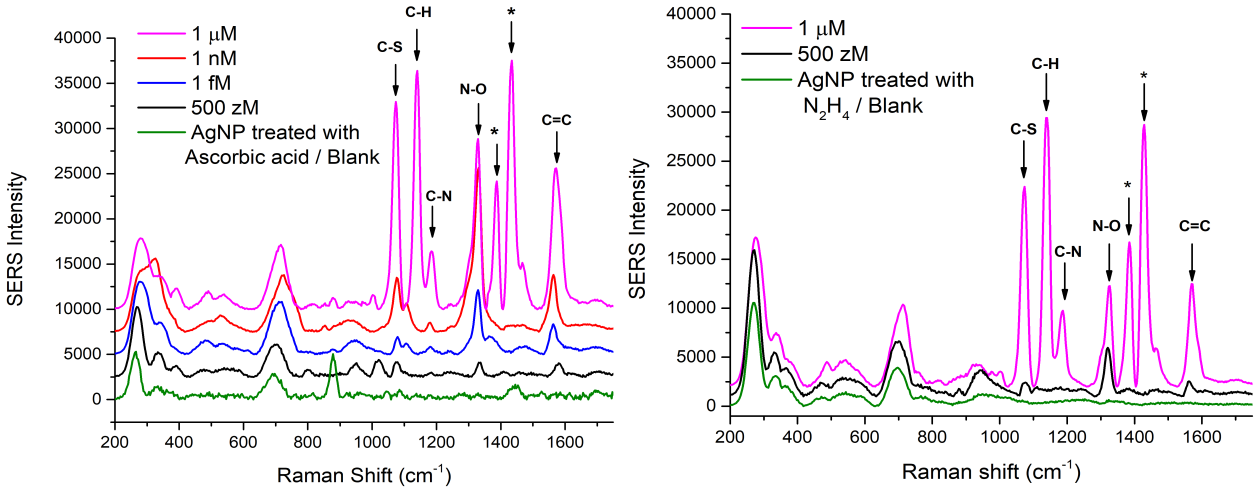

Figure S6. pNTP SERS spectra after oxygen removal using (left) ascorbic acid and (right) hydrazine. Vibrational modes originating from pNTP and AgNP treated with either ascorbic acid or hydrazine are given. In both systems the ring breathing vibrational mode is detected. NaOH was used to adjust the pH when ascorbic acid was used as an oxygen scavenger. Please note that the specific vibrations of pNTP were well visualized in the spectra ≥1100 cm^{-1} where there is less interference from the AgNP capping agents (citrate and ethanol) and the oxygen scavengers. Not all modes are observed at very low concentrations (500 zM).

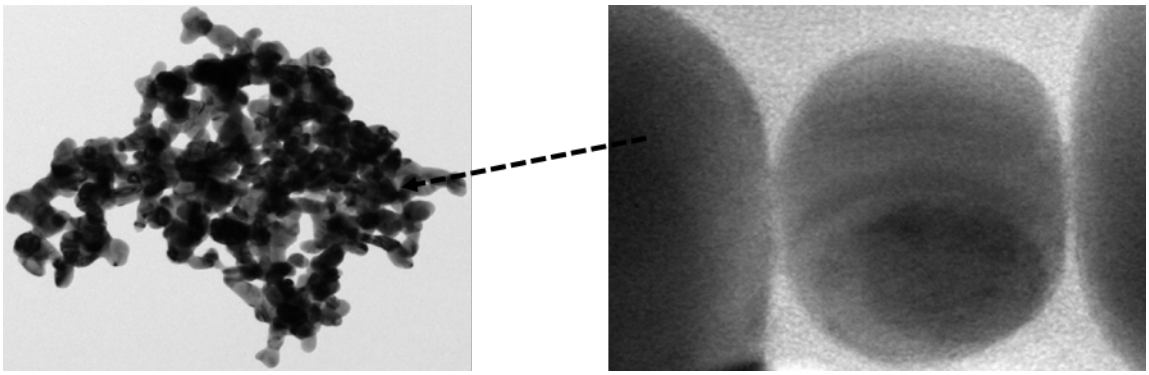

Figure S7. (left) A TEM image of AgNP aggregates formed during SERS detection and (right) a close up of nanogaps present within the aggregate.

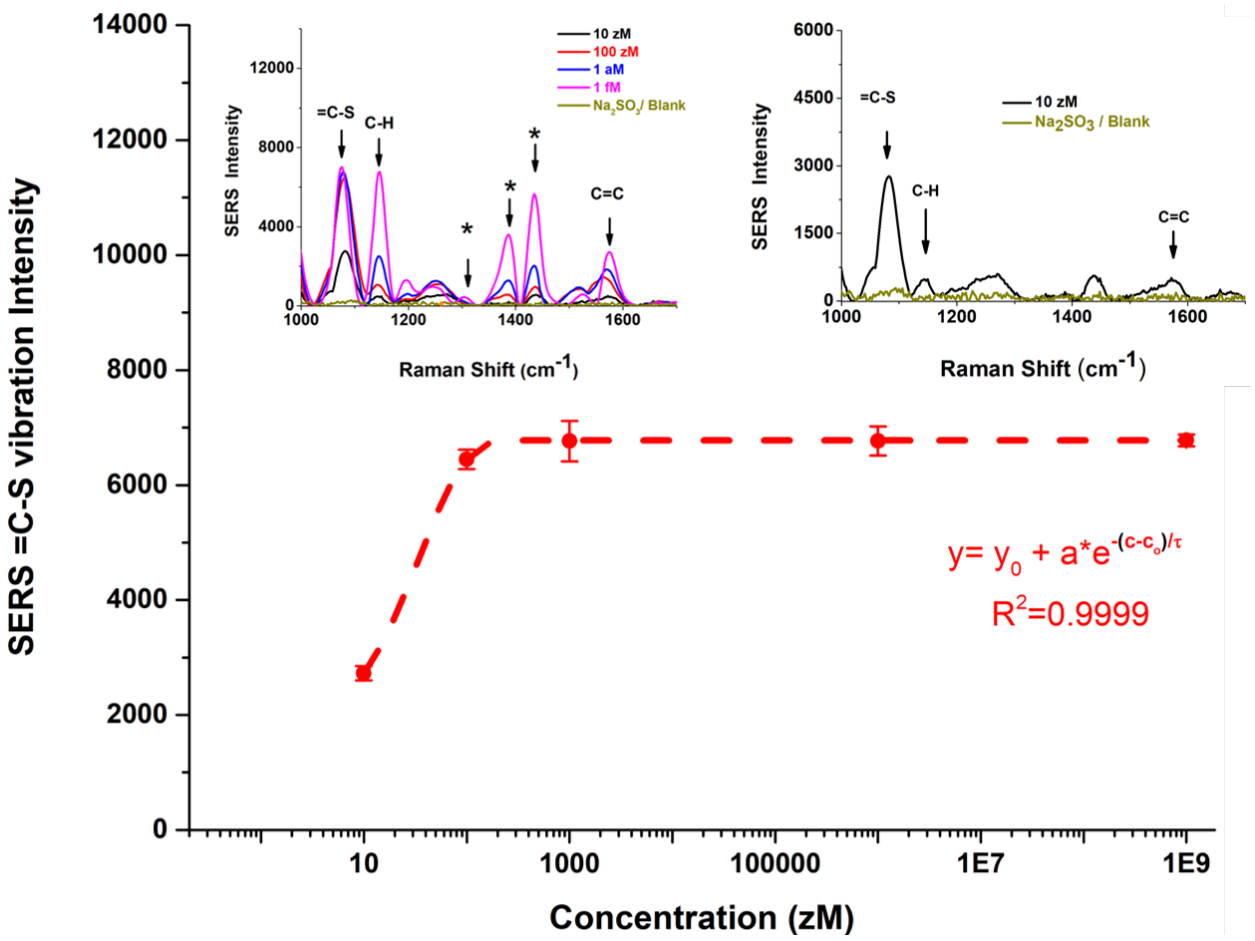

Figure S8. SERS signal intensity of the =C-S stretch in pATP after oxygen removal with Na_2SO_3. The insets show the pATP SERS spectrum at different concentrations and a comparison between a 10 zM pATP solution and the Na_2SO_3 containing blank. The characteristic pATP SERS signal displays a nonlinear increase in intensity of the =C-S vibrational mode, which can be attributed to S-AgNP bond out-of-plane vibration.

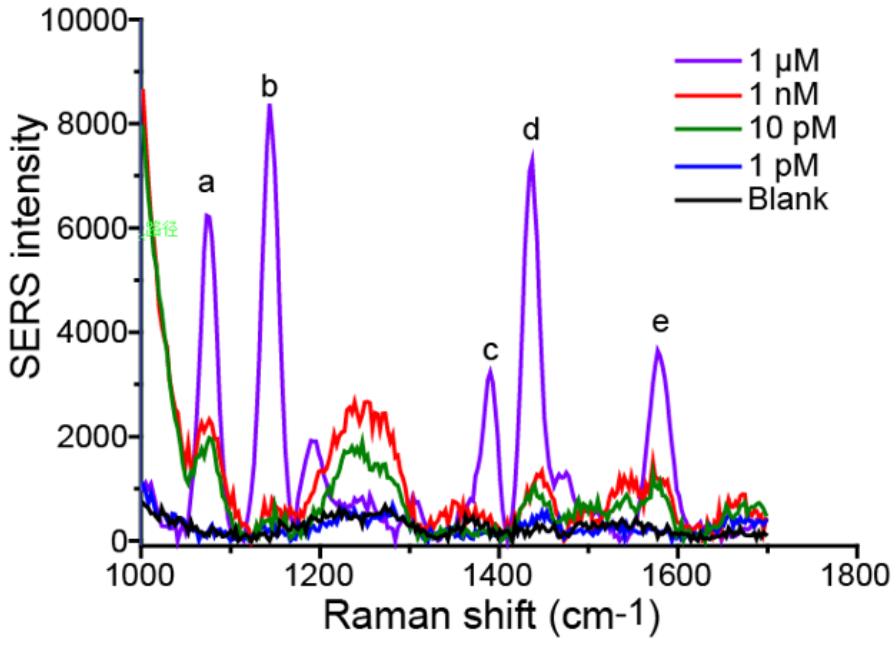

Figure S9. The SERS signal intensity of the =C-S stretch in pATP as the function of [pATP] without oxygen removal. Na_2SO_4 was used to aggregate the AgNPs and maintain the ionic strength of the sample solutions.

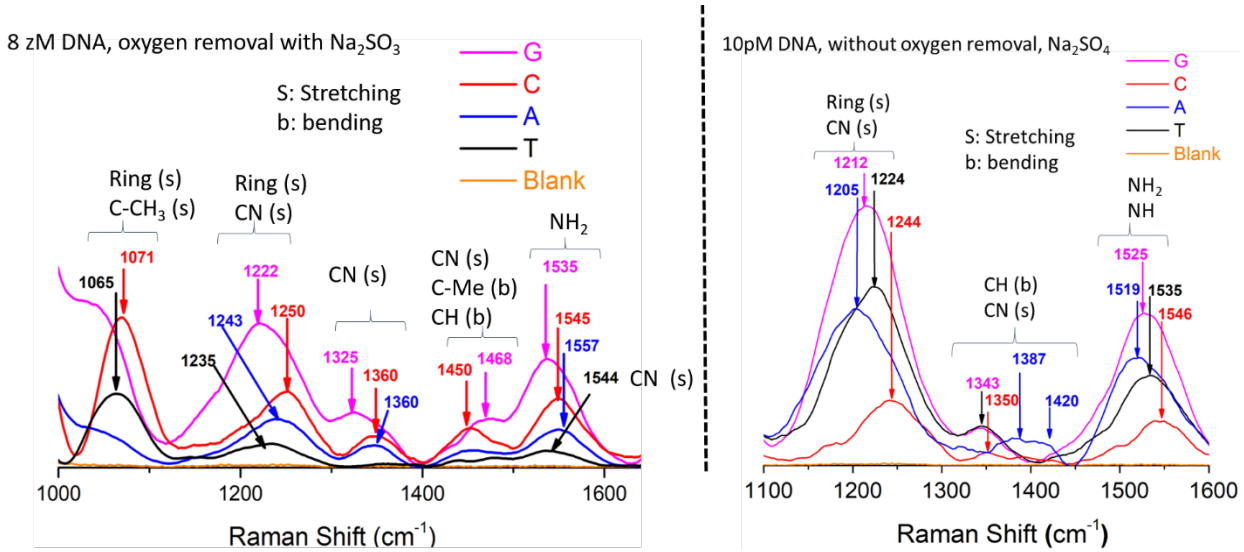

Figure S10. The SERS spectra of four homopolymeric oligoDNA sequences (left) with and (right) without oxygen removal. Strong signals from the capping molecules, i.e., citrate and ethanol, obscure any DNA vibration modes <1000 cm^{-1}. In the absence of dissolved oxygen significant distinction appears between some vibrational modes, e.g., the pyrimidine ring stretching at 1071 cm^{-1}. Spectra were only recorded ≥1100 cm^{-1} under aerobic conditions to allow clear visualization of the vibration modes. Not all modes are observed at such low concentrations.

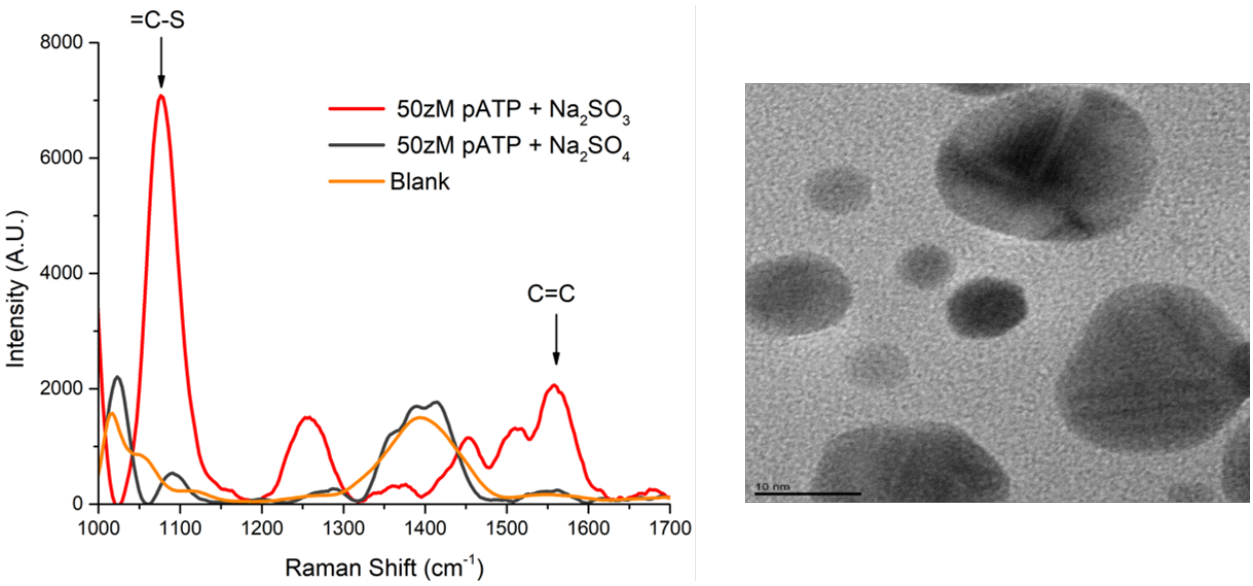

Figure S11. (left) The SERS spectra of pATP obtained using spherical AgNPs with and without oxygen removal. (right) A TEM picture of the spherical AgNPs.

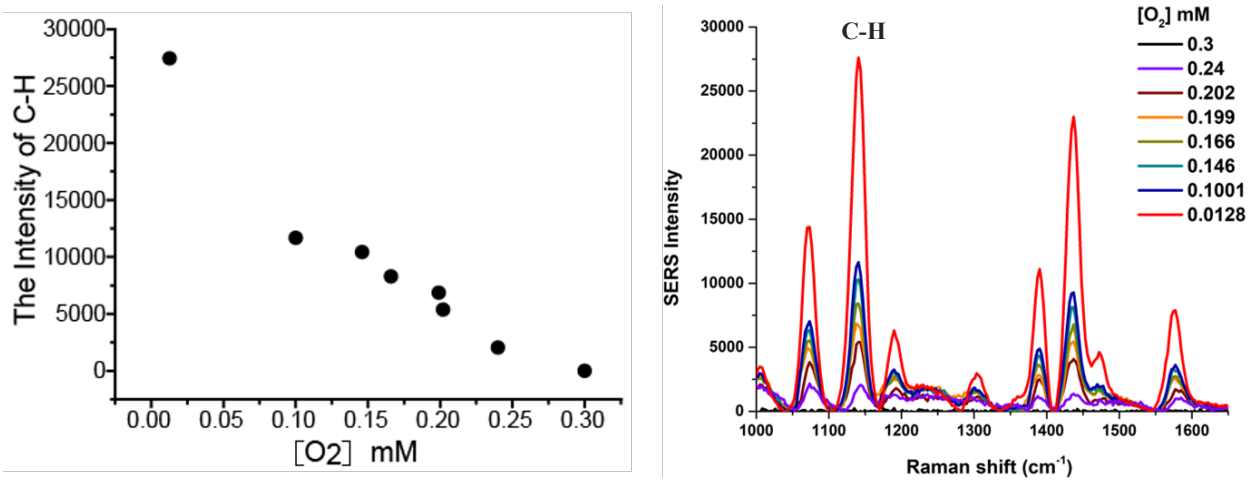

Figure S12. Quantitative correlation between SERS signal intensity of the C-H stretching band (1130 cm^{-1}) and dissolved oxygen concentrations obtained by N_2 sparging.

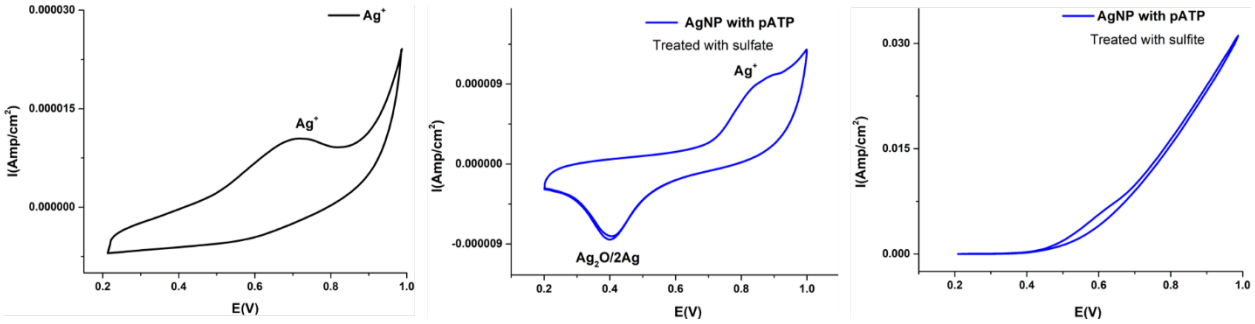

Figure S13. Cyclic voltammograms of $AgNO_3$ and AgNPs with pATP adsorbed on their surface. a) $AgNO_3$, and AgNPs with pATP in b) the presence and c) absence of dissolved oxygen. The Ag_2O layer disappears in absence of dissolved oxygen. A AgIAgCl external reference electrode was used in this experiment.

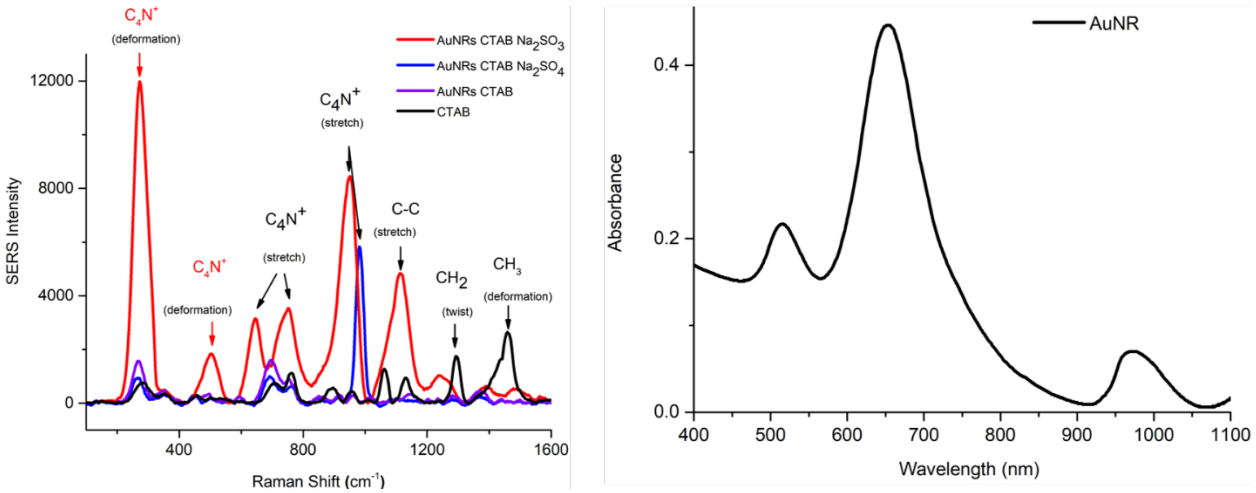

Figure S14. (left) The SERS spectra of gold nanorods (AuNRs) capped with cetyltrimethylammonium bromide (CTAB). Different C_4N^+ vibrational modes (2 deformations and 3 stretches) are detected in absence of dissolved oxygen. (right) The visible absorbance spectrum of the AuNRs.

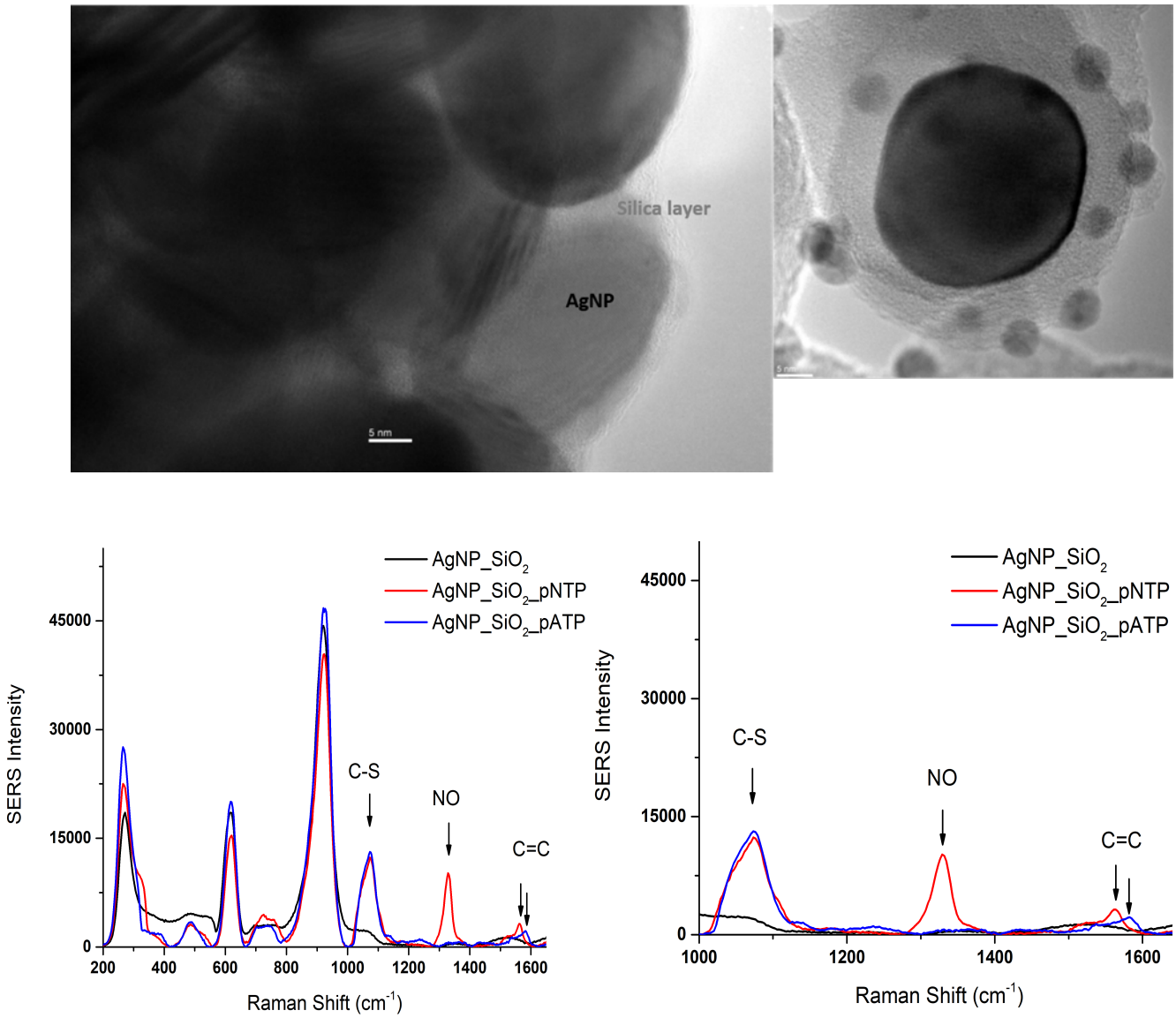

Figure S15. TEM images of SiO_2-coated AgNPs and SERS spectra of SiO_2-coated AgNP blanks and in the presence of pNTP and pATP. The analytes are adsorbed to the 3±1 nm thick SiO_2 layer.

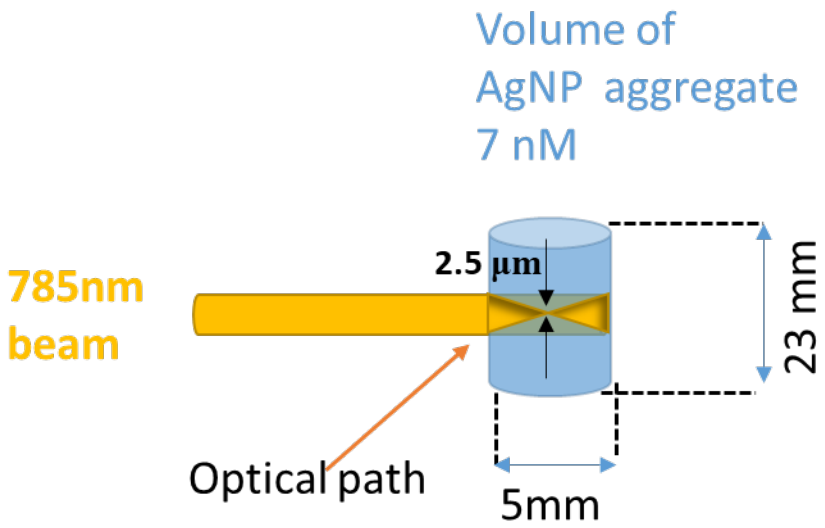

Figure S16. Scheme illustrating the size of the incident light beam relative to the total sample size. The probability of the analyte molecule existing within the irradiated volume was calculated to be 5.4x 10^{-8}:1 based on the volume ratio of the light path to the sample, assuming the analyte molecule is homogeneously distributed.

Calculation of the probability (p) is based on the following equation:

$$p = \frac{V_i}{V_s} = \frac{3.14\times\left(\frac{2.5}{2}\right)^2\times 5000}{3.14\times\left(\frac{5000}{2}\right)^2\times 23000} = 5.4\times 10^{-8}$$

Where p is the percentage of the sample that was irradiated by the incident light, V_i is the sample volume (μm^3) that was irradiated, and V_s is the total sample volume (μm^3).

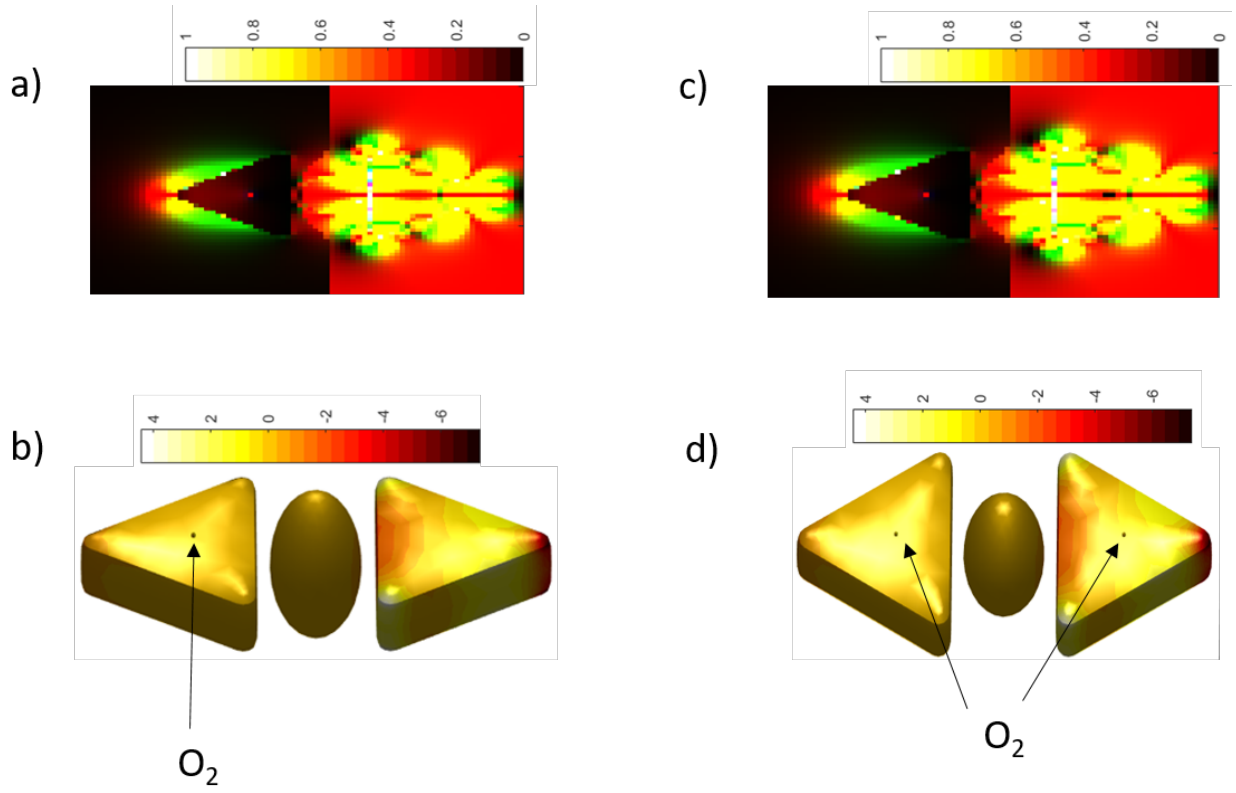

Figure S17. a) The electromagnetic field distribution surrounding an aggregate containing one spherical AgNP between two nanoprisms in aqueous solution with one oxygen molecule on the left prism and b) its corresponding charge distribution. c) The electromagnetic field distribution with one oxygen molecule on each nanoprism and d) its corresponding charge distribution.

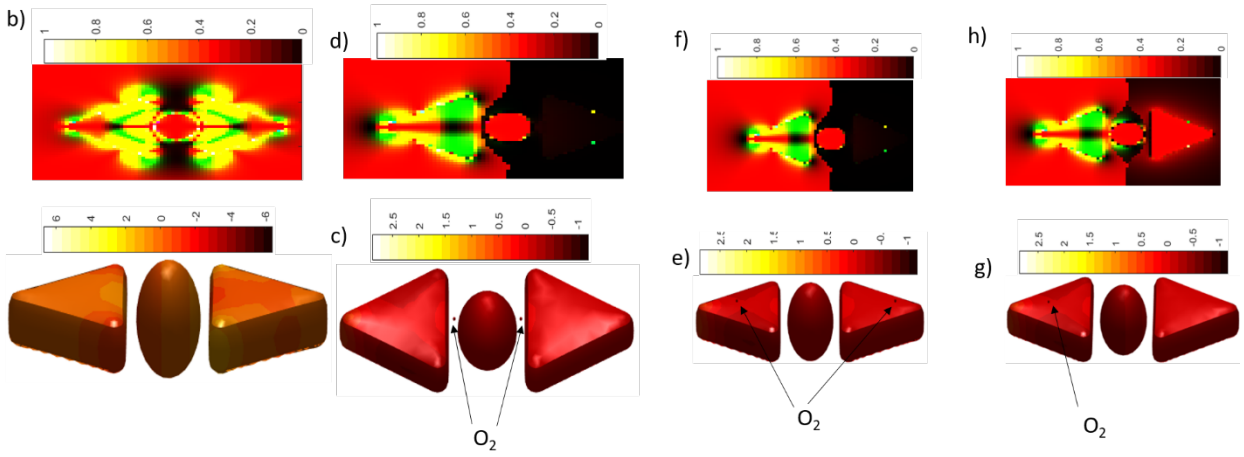

Figure S18. The electromagnetic field distribution of an aggregate that contains one spherical AgNP between two nanoprisms in aqueous solution. The AgNPs are coated with a 3 nm thick Ag_2O layer. a) without dissolved oxygen, b) with one oxygen molecule within each nanogap, c) with one oxygen molecule on each nanoprism, and d) with one oxygen molecule on the left nanoprism. e), f), g), and h) are the corresponding charge distributions for a), b), c), and d), respectively.

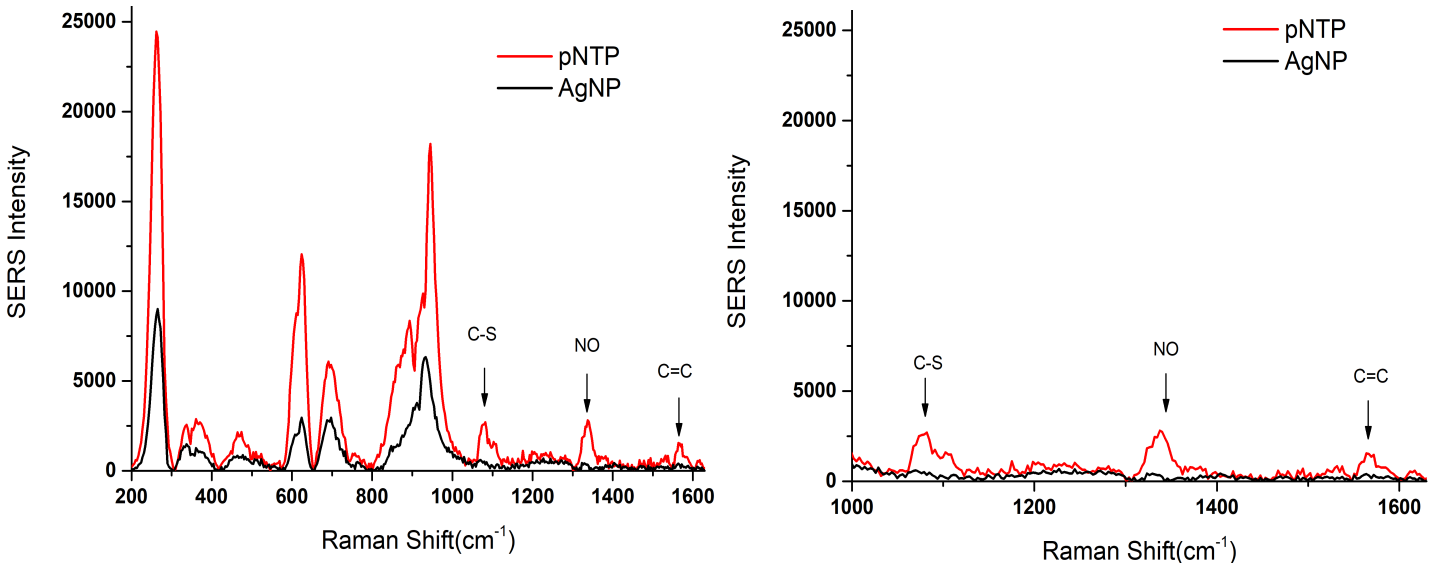

Figure S19. The SERS spectra of pNTP covalently bound to a silver mirror surface at the bottom of a quartz NMR tube ~10 cm from the incident light source (red). The corresponding spectrum of the AgNP blank (black). Both samples are treated with Na_2SO_3. The AgNP substrate capping molecules have strong signal interference <1000 cm^{-1}.

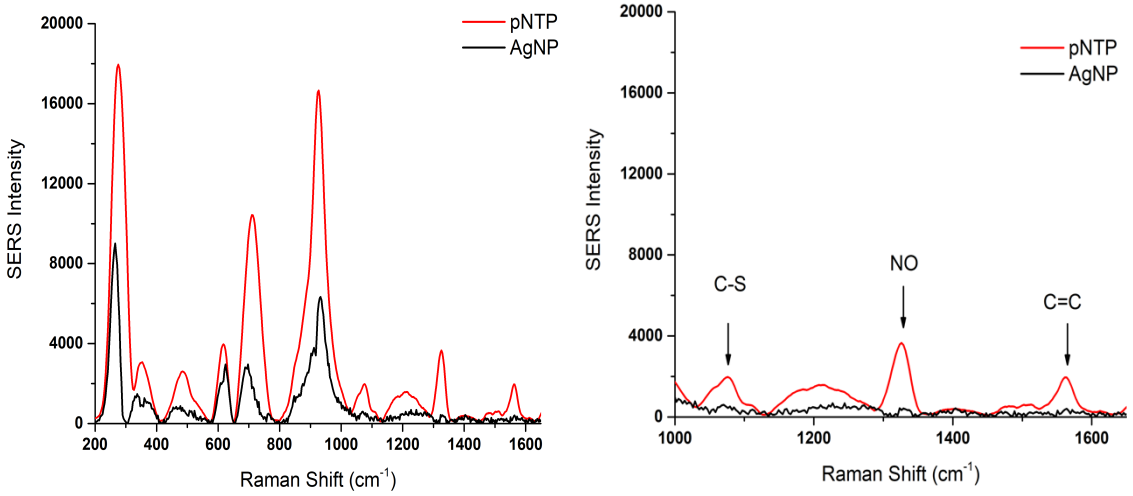

Figure S20. The SERS spectra of pNTP covalently bound to a silver mirror at the distal end of a 1 m long PEEK capillary tubing (red). The corresponding spectrum of the AgNP blank (black). Both samples were treated with Na_2SO_3. The AgNP substrate capping molecules have strong signal interference <1000 cm^{-1}.

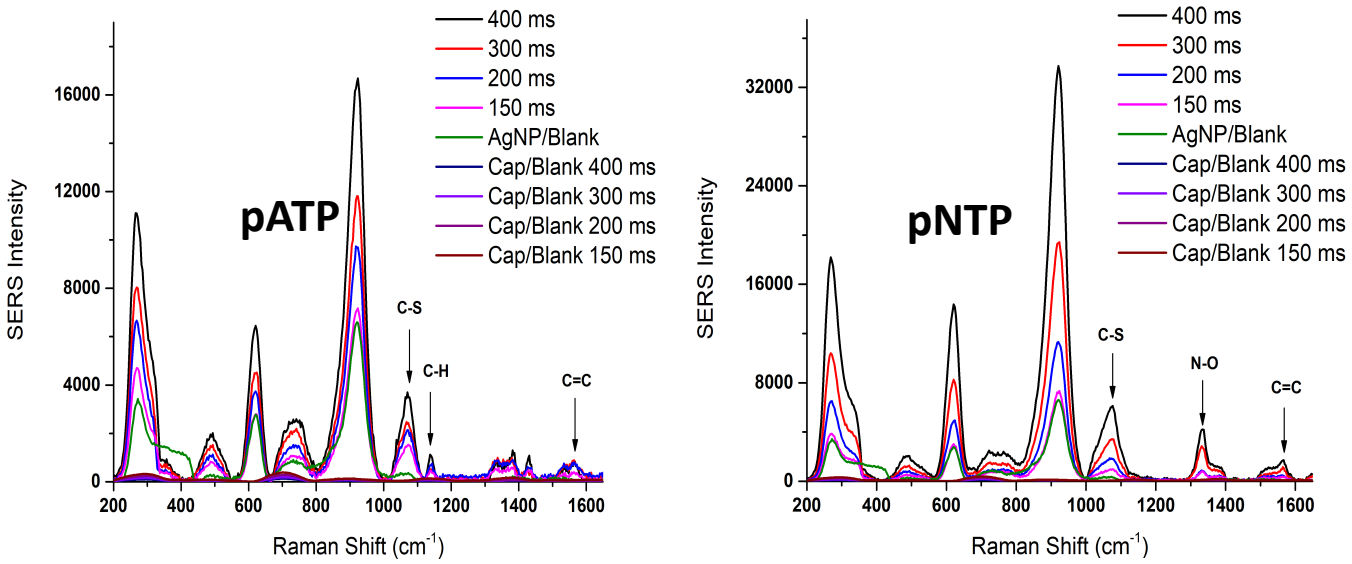

Figure S21. The SERS spectra of pATP and pNTP immobilized on a silver mirror surface on a 96-well plate for varying integration times (i.e., 150-400 milliseconds). A glass capillary tube filled with agglomerated deoxygenated AgNPs was dipped in the 96-well plate containing AgNP-pATP or AgNP-pNTP and the SERS signal was measured remotely from the mirror surface. The signal intensity was >1000 counts with negligible contribution from the glass capillary (capillary blanks are given for varying integration times too.

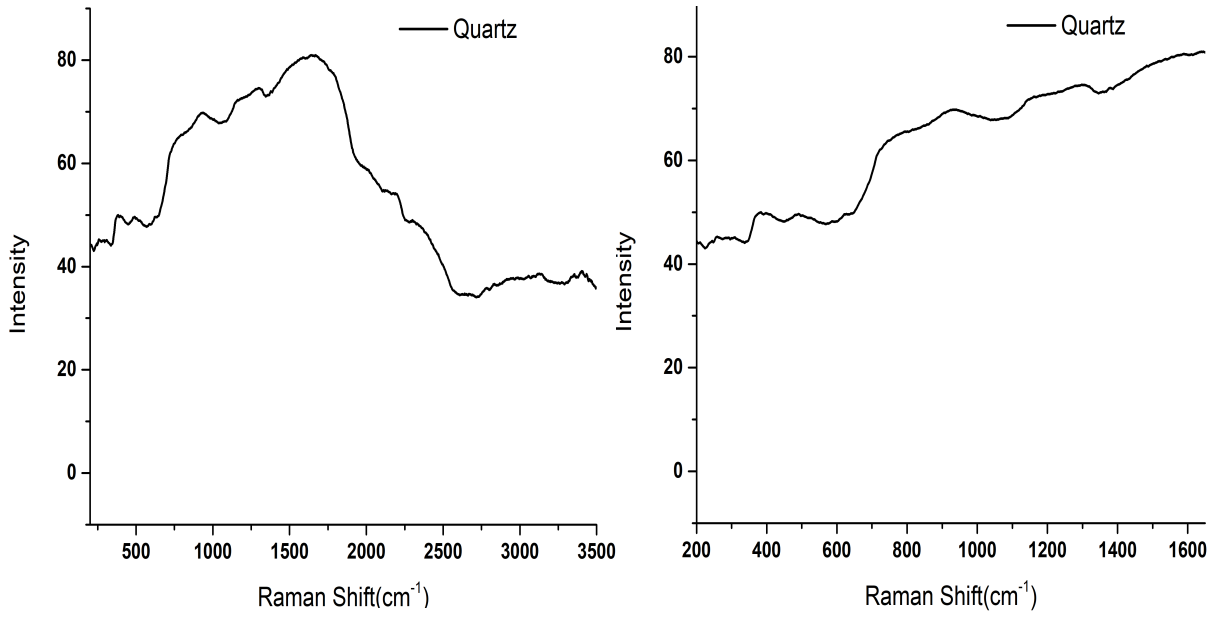

Figure S22. The background spectra of the quartz sample holder. Note: The signal intensity is <100 counts.

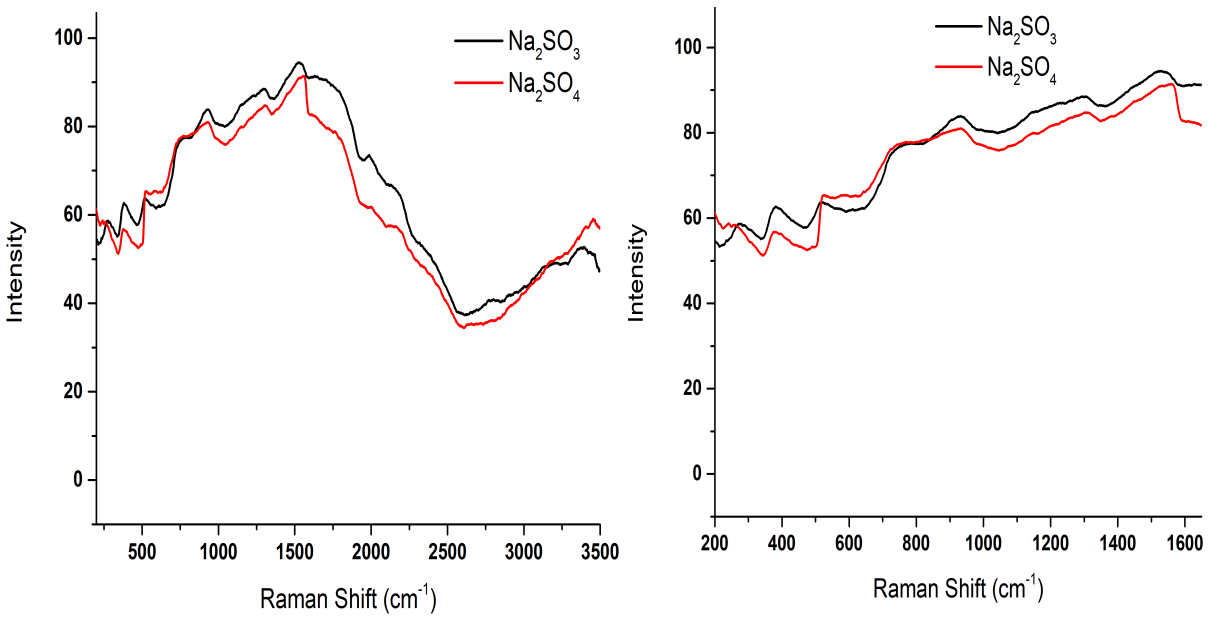

Figure S23. The spectra of aqueous Na_2SO_3 and Na_2SO_4. Note: The signal intensity is <100 counts.

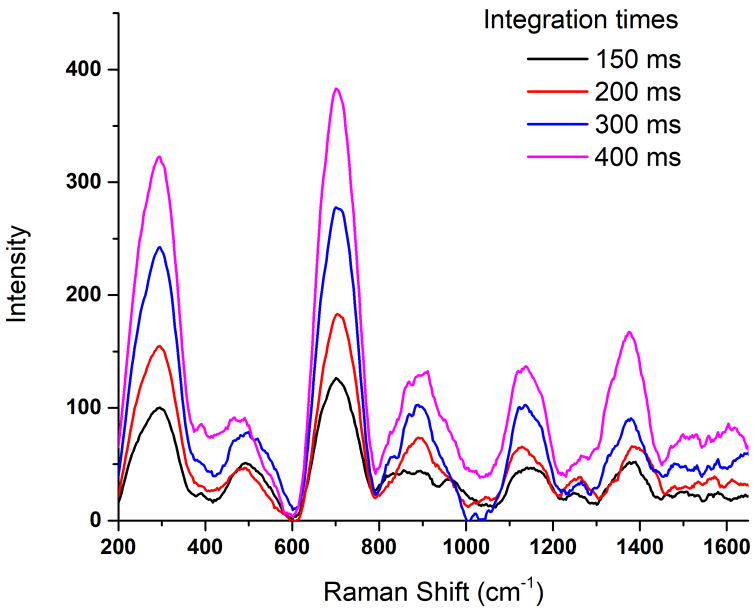

Figure S24. The spectrum of a glass capillary tube at different integration times. Note: The signal intensity is <500 counts.

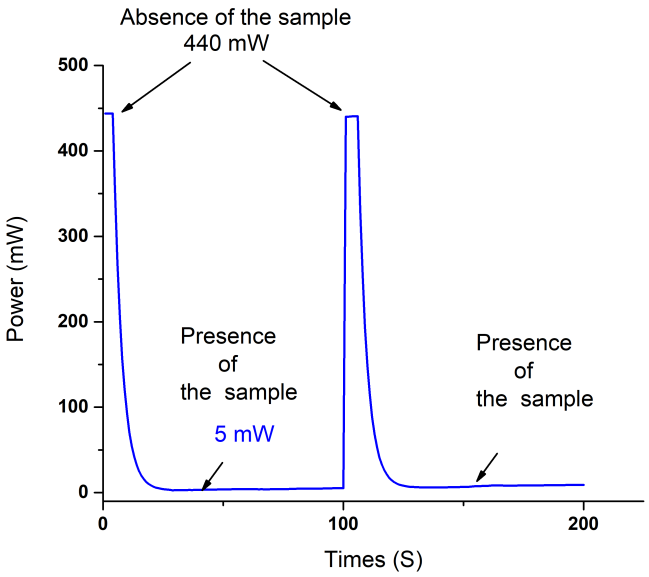

Figure S25. Laser power evolution on the substrate in the presence and absence of the sample. The 450 mW source emits ~440 mW at the lens of the fiber optic bundle, of which ~ 5 mW reached the sample.

Table S1. The oligoDNA sequences being detected by SERS.

Homopolymer oligo DNA	Sequences (5'→ 3')
5G	HS-GGGGG
5C	HS-CCCCC
5A	HS-AAAAA
5T	HS-TTTTT

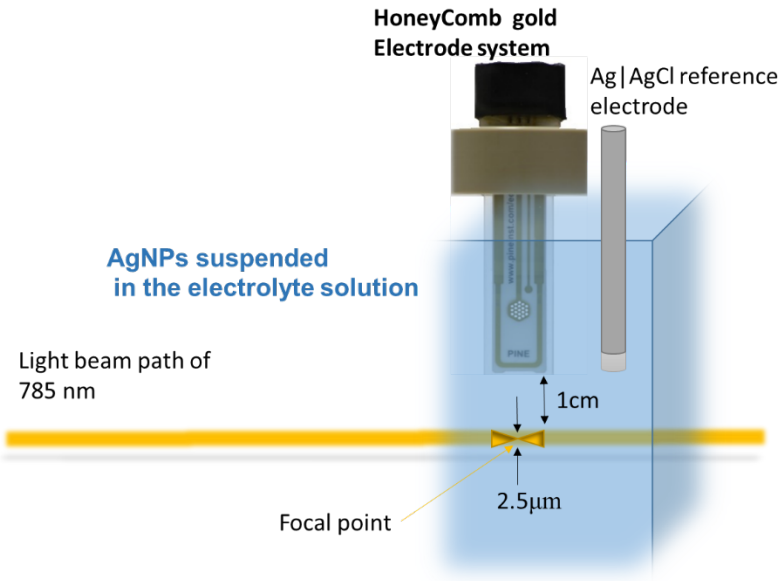

Scheme S1. The photoelectrochemical measurement apparatus where the blue represents suspended AgNPs. The electrolyte is either Na_2SO_4 or Na_2SO_3 at constant ionic strength.

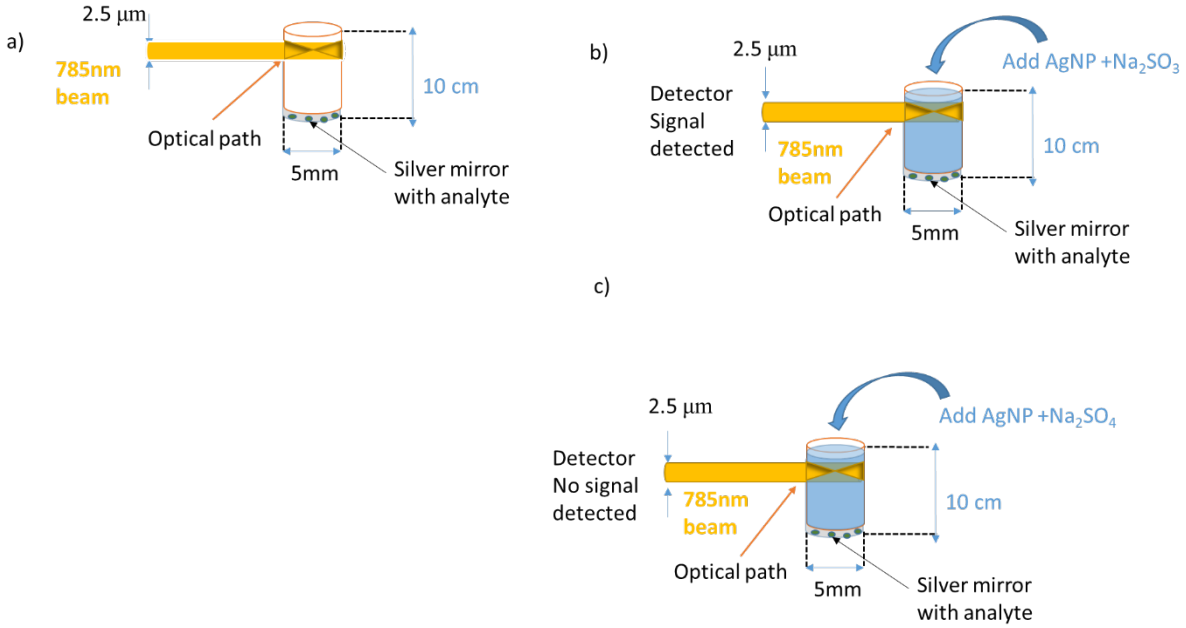

Scheme S2. Remote sensing of pATP adsorbed onto a silver mirror 10 cm away from the optical path of the instrument. a) The analyte is adsorbed onto a silver mirror and AgNP suspensions are added and agglomerated with either b) Na_2SO_3 or c) Na_2SO_4. Signal was observed in the absence of dissolved oxygen, but not in its presence. It is unlikely that an analyte adsorbed on the silver mirror will desorb and diffuse against the direction of flow to readsorb on an upstream AgNP.

References

1 Zhang, Q., Li, N., Goebl, J., Lu, Z. & Yin, Y. A Systematic Study of the Synthesis of Silver Nanoplates: Is Citrate a "Magic" Reagent? *Journal of the American Chemical Society* **133**, 18931-18939, doi:10.1021/ja2080345 (2011).

2 Hohenester, U. & Krenn, J. Surface plasmon resonances of single and coupled metallic nanoparticles: A boundary integral method approach. *Physical Review B* **72**, 195429, doi:10.1103/PhysRevB.72.195429 (2005).

3 García de Abajo, F. J. & Howie, A. Relativistic Electron Energy Loss and Electron-Induced Photon Emission in Inhomogeneous Dielectrics. *Physical Review Letters* **80**, 5180-5183, doi:10.1103/PhysRevLett.80.5180 (1998).

4 García de Abajo, F. J. & Howie, A. Retarded field calculation of electron energy loss in inhomogeneous dielectrics. *Physical Review B* **65**, 115418, doi:10.1103/PhysRevB.65.115418 (2002).

5 Lagos, M. J., Trügler, A., Hohenester, U. & Batson, P. E. Mapping vibrational surface and bulk modes in a single nanocube. *Nature* **543**, 529, doi:10.1038/nature21699 (2017).

6 Hohenester, U. & Trugler, A. Interaction of Single Molecules With Metallic Nanoparticles. *IEEE Journal of Selected Topics in Quantum Electronics* **14**, 1430 - 1440, doi:10.1109/JSTQE.2008.2007918.

7 García de Abajo, F. J. Optical excitations in electron microscopy. *Reviews of Modern Physics* **82**, 209-275, doi:10.1103/RevModPhys.82.209 (2010).

8 Johnson, P. B. & Christy, R. W. Optical Constants of the Noble Metals. *Physical Review B* **6**, 4370-4379, doi:10.1103/PhysRevB.6.4370 (1972).

9 Saroja, G., Vasu, V. & Nagarani, N. Optical Studies of Ag2O Thin Film Prepared by Electron Beam Evaporation Method. *Open Journal of Metal* **3** (2013).

10 COMMERCE, U. S. D. O. & STANDARDS, N. B. O. Table of Dielectric Constants of Pure Liquids. *National Bureau of Standards Circular* **514** (1951).